PLASMA DYNAMICS

VI. PLASMAS AND CONTROLLED NUCLEAR FUSION*

C. Plasma Diagnostics

Academic and Research Staff

Prof. G. Bekefi
Prof. E. V. George
Dr. P. A. Politzer

1. STARK PROFILES OF FORBIDDEN AND ALLOWED TRANSITIONS IN A DENSE, LASER-PRODUCED HELIUM PLASMA

Introduction

The Stark profile of an allowed spectral line interacting with a nearby forbidden transition has received much attention in recent years. Not only is this problem of basic theoretical interest but a thorough understanding of it will provide a powerful diagnostic method of determining plasma densities. Not only the linewidth of a Stark-broadened line but the intensity ratio and relative shift of the two components can be used in a sensitive determination of plasma density.

In the conventional theory[1-3] for the computation of a pair of interacting lines, the quasi-static approximation for the perturbing ions and the impact approximation for the perturbing free electrons are ordinarily used. Recent measurements[4, 5] have shown that agreement along the allowed line profile is generally good, but the forbidden line appears to be weaker and broader than predicted by theory. Burgess[4] suggests that ion dynamics, which is ignored in the quasi-static approximation, may be important in determining the profile around the forbidden line. Griem[6] shows that this is indeed so, and calculates in an approximate way the magnitude of the effect. The reduction of the peak intensity of the forbidden line caused by ion motions turns out to be quite appreciable and the effect is stronger, the lower the electron density and the higher the temperature.

In this report we present a theoretical and experimental study of a pair of neutral helium lines that have not been examined hitherto, the 6678 Å (2^1P-3^1D) allowed line and the 6632 Å (2^1P-3^1P) forbidden line. We discuss theory and computations, describe our experimental results, and make comparisons with theory.

Calculations of Line Profiles

a. Neglect of Ion Dynamics

The combined profile of the 2^1P-3^1D, 3^1P allowed and forbidden lines is calculated for a variety of electron densities and temperatures. Our method follows closely

*This work was supported by the U.S. Atomic Energy Commission (Contract AT(30-1)-3980).

Griem's computations[1] of the 2^3P-4^3D, 4^3F pair of helium lines; that is, the perturbing ions are treated in the quasi-static approximation and the perturbing electrons in the impact approximation. Only two states, 3^1D and 3^1P, are allowed to interact, and the effect of the 3^1S state is included as a correction.

Within the framework of the above-mentioned approximations, the Stark profile of a pair of allowed and forbidden lines is given by Eq. (16) of Griem's paper.[7] The distribution function of ion field strengths is taken from Hooper.[8] The matrix elements of the operator Φ, which describes the electron impact broadening, are calculated in the limit of high temperatures where the electrons induce a broadening but not a shift. This is certainly justified for transitions between the 3^1D and 3^1P states. For transitions 3^1P-3^1S the high-temperature approximation is rather poor, but the contribution of this transition is small enough to make the resulting error insignificant.

The influence of the 3^1S state is taken into account in the same way as Griem[1] did for the 4^3P state. Since this influence is appreciable only at high field strengths where the 3^1P and 3^1D states are well mixed, the 3^1S state is assumed to give rise to a quadratic Stark effect while interacting with the two overlapping 3^1P, 3^1D states (at any field strength). This interaction results in a shift of the 3^1D and 3^1P levels away from the 3^1S state and an increase in their intensity. For this Stark effect to be truly quadratic, the increase in intensity should be small, less than, say, 10%. We then find from Eq. (27) of Griem's paper[1] that the maximum permissible field (with the magnetic quantum number m = 0) is approximately 5000 CGS units. If this field is taken to be ten times larger than the normal Holtsmark field, $E_0 = 2.61\, eN^{2/3}$, where e is the electron charge, and N the plasma density, it follows that $N \approx 3 \times 10^{17}$ cm^{-3}. This means that for densities less than this value, the assumption of a quadratic Stark effect is valid over ~95% of the area enclosed by the field distribution function. When the density exceeds 3×10^{17} cm^{-3}, the three states 3^1S, 3^1P, and 3^1D should be treated on an equal footing right from the beginning. Now a three-dimensional rather than a two-dimensional secular equation must be solved in order to determine the quasi-static shifts, and a three-dimensional matrix must be inverted to obtain the combined line profile arising from both electrons and ions.

The transition 2^1P-3^1S at 7281 Å is of no particular interest to us, since it is an allowed line in a spectral range not readily accessible to measurements; thus, its profile has not been calculated. Note, however, that the third level (4^3P) in Griem's work gives rise to the forbidden transition 2^3P-4^3P, and this reduces the intensity of the other two lines, 2^3P-4^3D, F. In our case, the third level gives rise to an allowed transition, the 2^1P-3^1S, which enhances the two other lines through its interaction with the 2^1P-3^1P forbidden transition.

Figure VI-1 illustrates the general features of the Stark profiles for different plasma densities. We see that as the density increases the two lines broaden and shift away

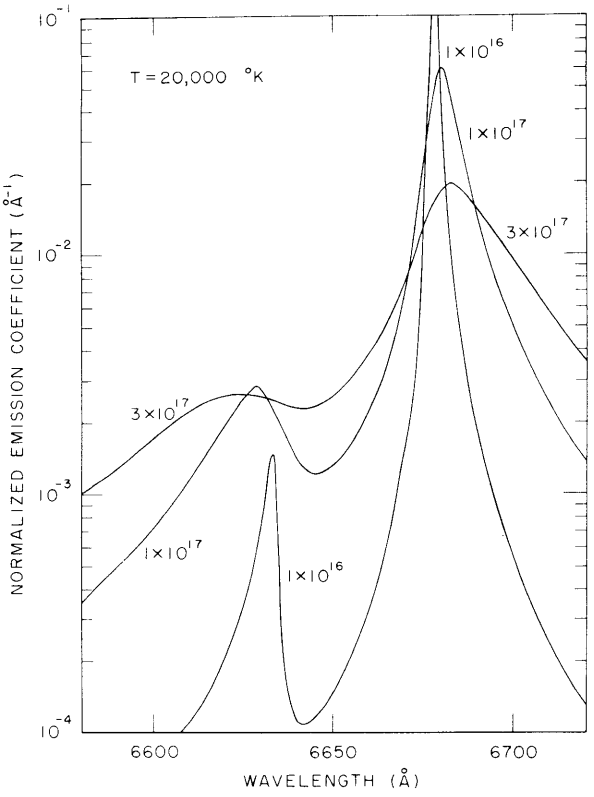

Fig. VI-1. Calculated Stark profile of the allowed 2^1P-3^1D line and the 2^1P-3^1P forbidden component of neutral helium, for three plasma densities, $N = 1 \times 10^{16}$, 1×10^{17} and 3×10^{17} cm^{-3}. Temperature, 20,000°K; total area under the combined lines is integrated to unity. For $N = 1 \times 10^{16}$ cm^{-3}, the peak intensity at ~6678 Å reaches a value equal to 0.68 $Å^{-1}$.

from one another, the shift of the forbidden line being the more pronounced. Also, the intensity of the forbidden line grows at the expense of the allowed line. The profiles shown in Fig. VI-1 are normalized to unity when integrated over both lines, except for a small correction (much less than 1%) caused by the interaction with the 3^1P state.

In summary, the main approximations in our calculations are: (i) the quasi-static approximation for the ions; (ii) the impact approximation for the electrons; (iii) the high-temperature approximation in the evaluation of the Φ matrix elements; (iv) neglect of the broadening of the lower 2^1P level, and (v) neglect of other intermediate states. Let us consider these one by one.

1. The quasi-static approximation holds for frequency separations $\Delta\omega$ from the line center in excess of the reciprocal of the average ion collision time, $\tau_i \approx N^{-1/3}(M/\kappa T_i)^{1/2}$, where M is the ion mass, and T_i the ion temperature. This

Table VI-1. Normalized line-intensity profiles of the allowed 2^1P-3^1D neutral helium line and of the 2^1P-3^1P forbidden component. Doppler broadening is taken account of for plasma densities $N = 3\times10^{15}$ cm^{-3} and 1×10^{16} cm^{-3}. The intensities are given to three significant figures. The last number and the sign in front of it specifies the power of ten by which the intensity must be multiplied (for example, 0.345-3 means 0.345×10^{-3}).

λ (Å)	$N = 3\times10^{15}$ cm^{-3}			$N = 1\times10^{16}$ cm^{-3}		
	10000 °K	20000 °K	40000 °K	10000 °K	20000 °K	40000 °K
6590.00	0.142-4	0.137-4	0.131-4	0.489-4	0.474-4	0.456-4
6600.00	0.214-4	0.207-4	0.201-4	0.726-4	0.703-4	0.678-4
6610.00	0.346-4	0.336-4	0.327-4	0.118-3	0.115-3	0.112-3
6618.00	0.575-4	0.561-4	0.546-4	0.197-3	0.195-3	0.192-3
6620.00	0.678-4	0.664-4	0.648-4	0.233-3	0.231-3	0.228-3
6622.00	0.817-4	0.802-4	0.785-4	0.281-3	0.281-3	0.278-3
6624.00	0.102-3	0.100-3	0.985-4	0.352-3	0.354-3	0.352-3
6626.00	0.134-3	0.133-3	0.131-3	0.468-3	0.474-3	0.476-3
6627.00	0.159-3	0.158-3	0.156-3	0.556-3	0.568-3	0.572-3
6628.00	0.194-3	0.193-3	0.192-3	0.686-3	0.706-3	0.717-3
6629.00	0.253-3	0.253-3	0.252-3	0.887-3	0.925-3	0.950-3
6630.00	0.368-3	0.372-3	0.372-3	0.124-2	0.132-2	0.138-2
6631.00	0.720-3	0.742-3	0.757-3	0.180-2	0.198-2	0.219-2
6632.00	0.594-3	0.602-3	0.584-3	0.121-2	0.129-2	0.134-2
6633.00	0.725-4	0.696-4	0.626-4	0.404-3	0.405-3	0.380-3
6634.00	0.386-4	0.360-4	0.317-4	0.218-3	0.212-3	0.194-3
6635.00	0.297-4	0.271-4	0.235-4	0.154-3	0.147-3	0.132-3
6640.00	0.255-4	0.223-4	0.188-4	0.983-4	0.883-4	0.760-4
6645.00	0.316-4	0.274-4	0.229-4	0.110-3	0.970-4	0.821-4
6650.00	0.428-4	0.369-4	0.309-4	0.144-3	0.125-3	0.105-3
6655.00	0.625-4	0.539-4	0.450-4	0.205-3	0.178-3	0.149-3
6660.00	0.101-3	0.869-4	0.724-4	0.326-3	0.282-3	0.235-3
6667.50	0.289-3	0.249-3	0.207-3	0.913-3	0.784-3	0.653-3
6670.00	0.490-3	0.422-3	0.351-3	0.153-2	0.131-2	0.109-2
6672.50	0.101-2	0.867-3	0.722-3	0.308-2	0.263-2	0.219-2
6673.75	0.165-2	0.142-2	0.118-2	0.494-2	0.422-2	0.350-2
6675.00	0.316-2	0.272-2	0.226-2	0.921-2	0.786-2	0.651-2
6676.25	0.842-2	0.722-2	0.601-2	0.230-1	0.196-1	0.162-1
6676.87	0.178-1	0.153-1	0.127-1	0.453-1	0.387-1	0.321-1
6677.00	0.220-1	0.188-1	0.156-1	0.544-1	0.465-1	0.387-1
6677.30	0.384-1	0.329-1	0.273-1	0.873-1	0.752-1	0.628-1
6677.60	0.847-1	0.726-1	0.604-1	0.160-0	0.141-0	0.120-0
6677.90	0.317-0	0.276-0	0.233-0	0.347-0	0.327-0	0.300-0
6678.10	0.143+1	0.132+1	0.112+1	0.552-0	0.564-0	0.568-0
6678.20	0.175+1	0.157+1	0.134+1	0.626-0	0.645-0	0.648-0
6678.30	0.146+1	0.131+1	0.121+1	0.648-0	0.677-0	0.684-0
6678.40	0.760-0	0.753-0	0.734-0	0.617-0	0.655-0	0.674-0
6678.50	0.436-0	0.421-0	0.400-0	0.553-0	0.591-0	0.622-0
6678.70	0.195-0	0.185-0	0.173-0	0.396-0	0.416-0	0.433-0
6679.00	0.852-1	0.800-1	0.739-1	0.232-0	0.235-0	0.235-0
6679.37	0.426-1	0.398-1	0.367-1	0.133-0	0.132-0	0.128-0
6680.00	0.190-1	0.177-1	0.163-1	0.637-1	0.619-1	0.592-1
6681.25	0.699-2	0.653-2	0.603-2	0.242-1	0.231-1	0.218-1
6682.50	0.364-2	0.340-2	0.315-2	0.126-1	0.120-1	0.113-1
6685.00	0.152-2	0.142-2	0.132-2	0.519-2	0.491-2	**0.459-2**
6687.50	0.829-3	0.775-3	0.721-3	0.282-2	0.267-2	**0.250-2**
6690.00	0.522-3	0.489-3	0.458-3	0.177-2	0.167-2	0.156-2

λ (Å)	$N = 3 \times 10^{16}$ cm^{-3}			$N = 1 \times 10^{17}$ cm^{-3}			$N = 3 \times 10^{17}$ cm^{-3}		
	10000 °K	20000 °K	40000 °K	10000 °K	20000 °K	40000 °K	10000 °K	20000 °K	40000 °K
6590.00	0.149-3	0.146-3	0.142-3	0.505-3	0.514-3	0.514-3	0.125-2	0.134-2	0.143-2
6600.00	0.221-3	0.218-3	0.213-3	0.740-3	0.764-3	0.776-3	0.161-2	0.174-2	0.189-2
6610.00	0.362-3	0.362-3	0.357-3	0.116-2	0.122-2	0.127-2	0.203-2	0.220-2	0.240-2
6618.00	0.614-3	0.626-3	0.630-3	0.171-2	0.186-2	0.201-2	0.232-2	0.247-2	0.267-2
6620.00	0.723-3	0.743-3	0.753-3	0.189-2	0.207-2	0.225-2	0.236-2	0.250-2	0.268-2
6622.00	0.869-3	0.903-3	0.924-3	0.207-2	0.227-2	0.250-2	0.239-2	0.252-2	0.268-2
6624.00	0.107-2	0.113-2	0.117-2	0.223-2	0.246-2	0.272-2	0.241-2	0.252-2	0.264-2
6626.00	0.137-2	0.146-2	0.154-2	0.234-2	0.257-2	0.286-2	0.241-2	0.249-2	0.259-2
6627.00	0.156-2	0.168-2	0.180-2	0.235-2	0.258-2	0.287-2	0.240-2	0.248-2	0.255-2
6628.00	0.178-2	0.194-2	0.211-2	0.234-2	0.256-2	0.282-2	0.239-2	0.246-2	0.251-2
6629.00	0.201-2	0.222-2	0.245-2	0.230-2	0.249-2	0.271-2	0.238-2	0.243-2	0.247-2
6630.00	0.216-2	0.240-2	0.270-2	0.222-2	0.238-2	0.256-2	0.237-2	0.241-2	0.242-2
6631.00	0.206-2	0.227-2	0.253-2	0.211-2	0.223-2	0.236-2	0.236-2	0.238-2	0.237-2
6632.00	0.162-2	0.173-2	0.182-2	0.198-2	0.207-2	0.214-2	0.234-2	0.235-2	0.233-2
6633.00	0.113-2	0.116-2	0.115-2	0.185-2	0.190-2	0.192-2	0.233-2	0.233-2	0.228-2
6634.00	0.806-3	0.810-3	0.771-3	0.171-2	0.174-2	0.172-2	0.232-2	0.230-2	0.224-2
6635.00	0.619-3	0.611-3	0.569-3	0.160-2	0.160-2	0.155-2	0.230-2	0.228-2	0.220-2
6640.00	0.357-3	0.332-3	0.294-3	0.124-2	0.119-2	0.108-2	0.229-2	0.221-2	0.206-2
6645.00	0.356-3	0.320-3	0.276-3	0.120-2	0.111-2	0.973-3	0.241-2	0.227-2	0.205-2
6650.00	0.433-3	0.382-3	0.325-3	0.136-2	0.122-2	0.105-2	0.269-2	0.248-2	0.219-2
6655.00	0.594-3	0.518-3	0.436-3	0.174-2	0.153-2	0.129-2	0.323-2	0.292-2	0.253-2
6660.00	0.913-3	0.789-3	0.660-3	0.249-2	0.215-2	0.180-2	0.417-2	0.371-2	0.318-2
6667.50	0.241-2	0.206-2	0.171-2	0.565-2	0.480-2	0.396-2	0.712-2	0.627-2	0.536-2
6670.00	0.391-2	0.333-2	0.276-2	0.835-2	0.708-2	0.584-2	0.884-2	0.783-2	0.677-2
6672.50	0.748-2	0.635-2	0.524-2	0.135-1	0.116-1	0.960-2	0.111-1	0.998-2	0.881-2
6673.75	0.115-1	0.973-2	0.801-2	0.180-1	0.155-1	0.131-1	0.124-1	0.113-1	0.101-1
6675.00	0.198-1	0.168-1	0.139-1	0.245-1	0.217-1	0.187-1	0.139-1	0.128-1	0.117-1
6676.25	0.415-1	0.357-1	0.298-1	0.339-1	0.313-1	0.282-1	0.153-1	0.143-1	0.134-1
6676.87	0.666-1	0.587-1	0.502-1	0.395-1	0.375-1	0.350-1	0.160-1	0.151-1	0.143-1
6677.18	0.873-1	0.786-1	0.689-1	0.425-1	0.409-1	0.390-1	0.164-1	0.155-1	0.148-1
6677.50	0.116-0	0.109-0	0.991-1	0.455-1	0.445-1	0.433-1	0.167-1	0.159-1	0.153-1
6677.81	0.151-0	0.148-0	0.144-0	0.483-1	0.480-1	0.476-1	0.171-1	0.163-1	0.157-1
6678.12	0.186-0	0.192-0	0.200-0	0.509-1	0.513-1	0.519-1	0.174-1	0.167-1	0.162-1
6678.74	0.209-0	0.227-0	0.251-0	0.550-1	0.569-1	0.595-1	0.179-1	0.174-1	0.170-1
6679.37	0.167-0	0.179-0	0.194-0	0.573-1	0.603-1	0.645-1	0.185-1	0.180-1	0.179-1
6680.00	0.118-0	0.125-0	0.131-0	0.576-1	0.612-1	0.661-1	0.189-1	0.186-1	0.186-1
6681.25	0.610-1	0.624-1	0.632-1	0.531-1	0.569-1	0.616-1	0.195-1	0.194-1	0.197-1
6682.50	0.353-1	0.355-1	0.352-1	0.456-1	0.487-1	0.524-1	0.197-1	0.198-1	0.204-1
6685.00	0.156-1	0.154-1	0.150-1	0.311-1	0.329-1	0.348-1	0.191-1	0.195-1	0.204-1
6687.50	0.865-2	0.844-2	0.811-2	0.213-1	0.223-1	0.232-1	0.176-1	0.182-1	0.192-1
6690.00	0.545-2	0.528-2	0.504-2	0.150-1	0.156-1	0.160-1	0.157-1	0.164-1	0.173-1

requirement ($\Delta\omega\tau_i \gg 1$) is almost always satisfied, except close to the line center where electron collisions or the Doppler effect often dominate. Note, however, that this argument cannot be extended to the case of forbidden lines for a reason that will be discussed.

2. The classical path impact approximation for electrons is valid when the average angular momentum quantum number ℓ for colliding electrons,[9] given by $N^{-1/3}(m\kappa T_e)^{1/2}/\hbar$, is much larger than unity. For conditions covered in Fig. VI-1 and Table VI-1, ℓ varies between 25 and 200, and the inequality $\ell \gg 1$ is fully satisfied. A second condition[9] for the validity of the classical path impact approximation is that strong collisions (with small ℓ) contribute little to the broadening. In other words, $R \equiv n^2\hbar\Delta\omega/\kappa T \ll 1$, where n is the principal quantum number of the upper level. For $\kappa T \approx 2$ eV, the approximation begins to deteriorate ($R \gtrsim 0.1$) for separations from the line center exceeding ~70 Å. Thus no significant errors are expected except, perhaps, at low temperatures and large frequency excursions $\Delta\omega$, where the profile is probably not measurable because the density is also low.

3. Errors attributable to the high-temperature approximation in the evaluation of the ϕ matrix are always smaller than approximately 10%. We infer this from the more exact calculation of electron impact broadening of Griem and co-workers.[10]

4. The broadening of the lower level of the transition (2^1P), which also causes broadening of the resonance line 1^1S-2^1P, contributes only a few percent to the total line broadening and thus can be safely neglected.

5. Finally, omission of other intermediate states (for example, with n = 4) should cause only small errors. This judgment is based on the fact that a similar omission of states with n = 3 in line-profile calculations of states with levels n = 4 likewise caused small errors.[1]

Thus, on the basis of these estimates, we believe that we are justified in claiming that the errors in the computed line profiles do not exceed 10%, on a par with other calculations of this kind.

b. Effect of Ion Dynamics on the Forbidden Line

The total integrated intensity of the forbidden line is determined mainly by the perturbing ions which have been hitherto treated quasi-statically. The colliding electrons, on the other hand, spread out the line and determine its shape. Recently, Burgess[4] suggested that ion motions may be important at and near the peak of the forbidden line. This effect is expected to be more prominent at low plasma densities where the line is narrower; here the frequency range around the peak where dynamic effects are important constitutes a larger portion of the line shape (the range $\Delta\omega$ over which the impact approximation applies varies as $N^{1/3}$, whereas the linewidth varies as N).

There is still no comprehensive theory that properly includes the dynamics of the ions. Recently, Griem[6] has calculated a forbidden-line profile in which the ions are

treated in the impact approximation; the plasma density is assumed to be sufficiently small that the linewidth of the forbidden line is much smaller than the frequency separation Δ between forbidden and allowed lines. The final profile is a convolution of profiles that are due to the electrons and the ions. The former is taken to be a dispersion profile of halfwidth w, which is the appropriate diagonal matrix element of the impact operation ϕ. The latter is calculated from the impact approximation of a single perturber (binary collision) in which the electron velocity is replaced by the ion velocity, and the ion temperature is assumed to equal the electron temperature.

The total integrated intensity of the forbidden line is then adjusted to be consistent with the quasi-static calculation described above. This means that ion collisions merely change the line shape but not its over-all intensity. In reality, the quasi-static ion shifts make the line asymmetric, but this effect is not considered in the present theory. Therefore only the gross features of the recalculated forbidden-line profile can be compared with the earlier theory or with experiment.

Subject to the above limitations, the "ion" profile of the forbidden line is given by

$$I(\omega) = (4r/\pi^2)(\Delta^2/\omega^2)\, a(|[\omega-\Delta]/\Delta|r). \tag{1}$$

The function $a(|z|)$ of Eq. 1 is defined as

$$a(|z|) = |z|\, K_o(|z|)\, K_1(|z|),$$

where K_o and K_1 are the modified Bessel functions of order zero and one. The parameter r is determined by the normalization procedure for the integrated line intensity discussed above; it is given by

$$r = 0.25\,(4R^2/3)^{1/4}\,[\pi M\hbar\Delta/m\kappa T]^{1/2},$$

with R as the radial matrix element between the two upper levels.

The effects of ion dynamics can now be found by comparing the final convolved line profile calculations made by means of Eq. 1, with the electron impact profile presented in Fig. VI-1. Since Eq. 1 does not allow for line asymmetry caused by ion static shifts, a detailed comparison of line shapes has no value. For that reason, we make comparisons at two characteristic points of the forbidden-line profile only. One is at the center (peak) value of the forbidden line; the other is at a wavelength situated midway between the unperturbed positions of the allowed and forbidden lines. Figure VI-2 illustrates the results of such calculations. For a given density and temperature, the ordinate value of each graph determines the numerical factor by which the intensity (of Fig. VI-1) must be multiplied to take proper account of ion dynamics. The upper graph of Fig. VI-2 refers to the correction appropriate to the peak of the forbidden line; the lower graph refers to the corresponding correction to be made midway

between the allowed and forbidden lines.

Figure VI-2 shows that ion motion lowers the peak intensity of the forbidden line and increases the intensity midway between allowed and forbidden lines. As expected, the

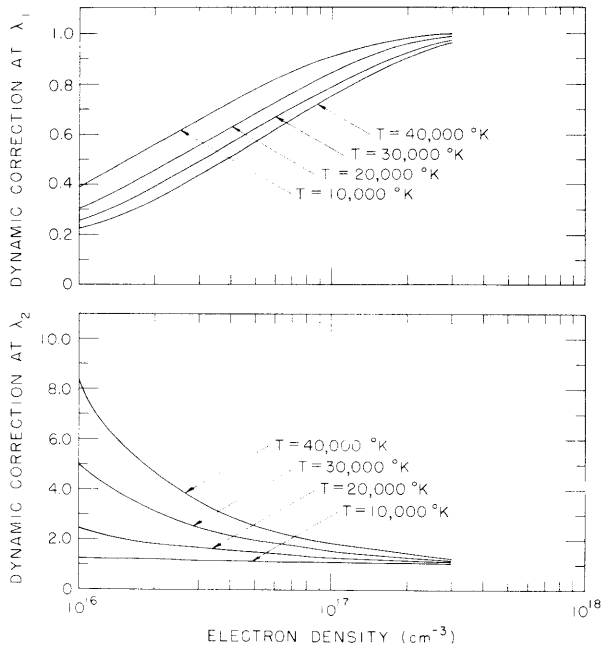

Fig. VI-2. Theoretical correction factors caused by ion dynamics, for different temperatures and densities, to be applied to the forbidden-line profiles calculated in Fig. VI-1. Upper graph refers to the correction that must be made at λ_1, the peak of the forbidden line; lower graph shows the corresponding correction at wavelength λ_2, which lies midway between the allowed and the forbidden lines.

effects are more pronounced, the lower the plasma density and the higher the temperature. For densities in excess of 10^{17} cm^{-3}, the corrections caused by ion motions are indeed small and Table VI-1 can be used as it is. At lower densities, and short of a complete theory which includes ion dynamics in a self-consistent way, the corrections imposed by Fig. VI-2 will henceforth be used in comparing theory with experiment.

Stark Profile Measurements of a Laser-Produced Plasma

The plasma produced by the relatively novel,[11] pulsed CO_2 laser is a very convenient spectroscopic source for plasma densities in the range 10^{15}-10^{19} cm^{-3}. Our laser produces 1-2 MW pulses of radiation at 10.6 μ wavelength. The pulse duration is

approximately 200 ns, and the repetition rate can be as high as 15 pps. This high repetition rate can be as high as 15 pps. This high repetition rate and good shot-to-shot reproducibility of the laser output permits spatial and temporal spectroscopic measurements of our plasma with good signal-to-noise ratio.

Figure VI-3 shows the experimental arrangement. The laser radiation is focused into a gas cell by means of a germanium lens of 3.8 cm focal length. The cell is filled with spectroscopically pure helium to a pressure of 3/4 atm. The light from the helium plasma generated by the laser pulses is focused onto the slits of a 0.5 m scanning spectrometer provided with a motor-driven wavelength scan (Jarrell-Ash, Model 82-020) and a photomultiplier output. The output signal from the photomultiplier is fed into a boxcar integrator (PAR Model 160) and then to graphic display equipment. The boxcar gate width is typically 250 ns, and thus represents the time resolution of our measurements. The gate can be set to any desired time delay relative to the time the laser is fired. This enables us to probe the entire afterglow history of the slowly decaying plasma. All measurements reported here, however, were made at a fixed time of 5 μs.

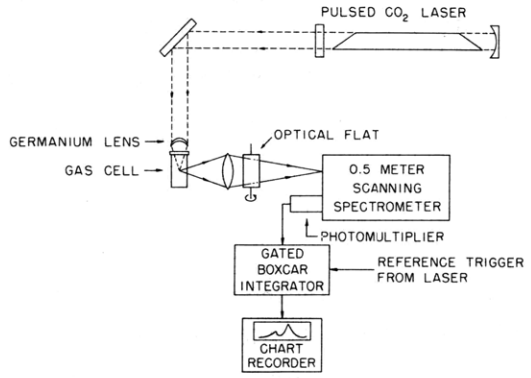

Fig. VI-3. Experimental arrangement.

Initially, the helium plasma is almost fully ionized ($N \sim 10^{19}$ cm^{-3}) and expands rapidly. At the time of our measurements (5 μs) the expansion has almost ceased and N has fallen to $\sim 10^{17}$ cm^{-3}. Now the plasma is roughly cigar shaped with the major axis pointing along the laser beam; it is 0.6 cm long and 0.2 cm in radius. Spatial resolution is achieved by placing an optical flat between the condensing lens and the spectrometer slits (see Fig. VI-3). Rotation of the flat focuses different radial regions of the plasma onto the entrance slit of the spectrometer. The slit height is typically 0.02 cm, and the slit width is ~20 μ. With a magnification of our condensing lens equal to ~2, a spatial resolution better than 0.01 cm is achieved.

Detailed spatial and temporal properties of the plasma will be reported elsewhere.[12] Here we need only point out that the plasma is quite symmetrical about the major axis of the plasma "cigar," and, therefore, Abel inversion of all our results is entirely

appropriate. For each spectral line examined, 20 lateral positions are obtained, and the results are Abel-transformed by means of a computer-generated program. This yields the desired line profiles as a function of radial distance from the plasma axis.

We have found that the neutral helium lines are emitted preferentially from the cool, outer cylindrical gas shell. The shell surrounds a hot, dense core that emits predominantly ionic lines. The plasma density within the outer shell is determined by measuring the Stark profile of the isolated 4713 Å HeI line. After Abel inversion of the results, each profile, corresponding to a given radial position r, is computer-fitted to the theoretical line profile.[13] Figure VI-4 illustrates a typical result for a radial position r = 0.11 cm. In this manner, the radial plasma density distribution is determined.

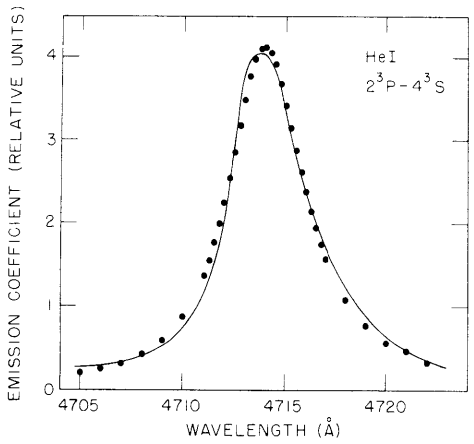

Fig. VI-4. Stark-broadened profile of the 2^3P-4^3S neutral helium line. Solid line refers to the Abel inverted experimental profile at a radial distance of 0.11 cm from the plasma axis; points represent the best fit with the theoretical profile with $N = 3.8 \times 10^{16}$ cm^{-3} and T = 34,000°K.

As is well known, the profile also depends somewhat on the electron temperature, and we deduce this quantity from the intensity ratio[14] of the following ionic and atomic lines: HeII (4686 Å) and HeI (5876 Å). We believe that we can measure plasma density to an accuracy of better than 15%. The measured apparatus width is generally much smaller than that of the observed lines and can usually be neglected. When this neglect is not justified, the measured linewidth has been corrected[15] appropriately. Also, at the time of observation (5 μs), self-absorption of all of the lines employed is found to be negligible, with the exception of the strong 5876 Å HeI line. To prove this, light emitted by the plasma in the direction away from the spectrometer slits is reflected back into the plasma by means of a spherical mirror. Measurement of the relative increase in the spectrometer output gives the absorptivity of the medium. The mild self-absorption observed for the 5876 Å line causes no serious difficulties. We do not use this line for density determination but only to obtain values of the electron temperature from the integrated line intensity. In this case even a substantial error in intensity causes but a minor error in the temperature.

Figure VI-5 shows a characteristic recorder output of the allowed and forbidden line

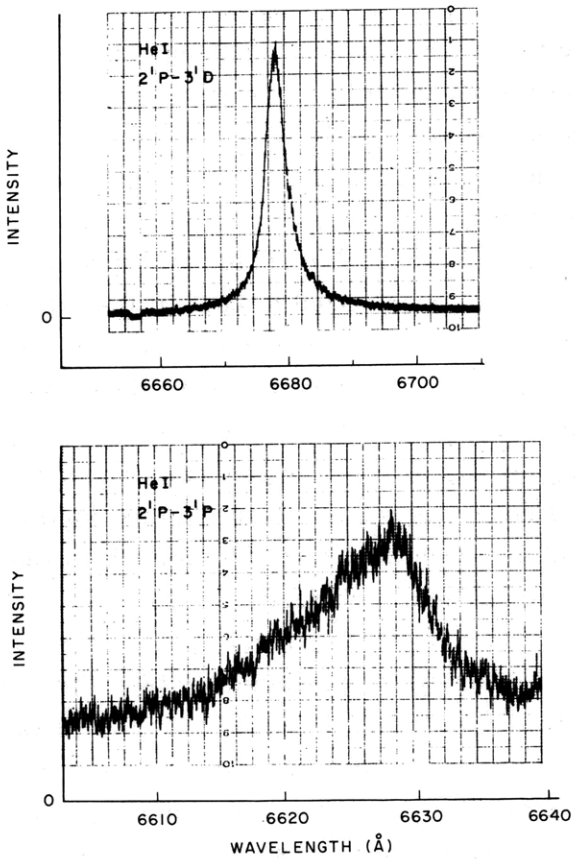

Fig. VI-5.

Measured intensity profile of the allowed line (above), and the forbidden line (below), at 5 μs in the afterglow of the laser-produced plasma, looking toward the plasma center. Intensity of the forbidden line is approximately 1/100 that of the allowed line. The change in sensitivity is achieved by changing the gain of the boxcar integrator (see Fig. VI-3) and by means of calibrated neutral density filters placed in front of the spectrometer slits.

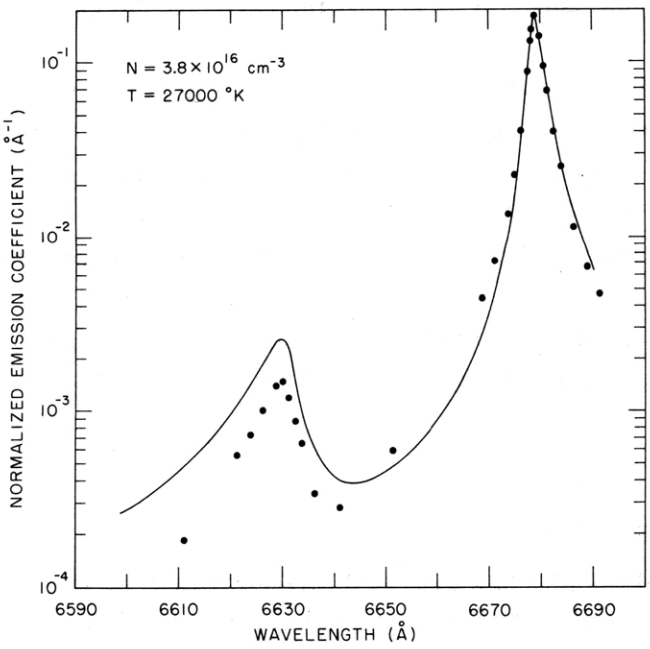

Fig. VI-6.

Allowed and forbidden line profiles at radial position r = 0.10 cm. Points represent Abel-inverted experimental results. The theoretical curves are chosen to give the best fit with experiment along the allowed line. The point to the far left of the graph, whose relative intensity is less than 3×10^{-4}, has substantial experimental errors and should not be judged on a par with the rest of the results.

combination obtained by looking straight toward the plasma center. Although the forbidden line intensity is only approximately 1% of the intensity of the allowed line, it is recorded with good discrimination and good signal-to-noise ratio.

Data like those shown in Fig. VI-5 are obtained for 20 different lateral positions, and are Abel-inverted. Figure VI-6 shows the results for a distance r = 0.10 cm measured from the plasma axis. The solid points refer to the Abel-inverted measurements. The lines represent theoretical profiles calculated and normalized to best fit the allowed line. We note that this fitting procedure yields still another independent value for the plasma density. It is reassuring that these densities agree within 15% with the densities deduced from the Stark-broadened 4713 Å HeI line (see Fig. VI-4).

We see from Fig. VI-6 that agreement along the allowed line is generally good, as expected, since there are no serious theoretical uncertainties in regard to this portion of the line profile. But we note quite substantial discrepancies along the forbidden line, similar to those found by earlier workers for other helium forbidden transitions.[4,5] The observed discrepancies between experiment and theory are more than a factor of two in intensity, and they cannot be removed merely by changing the plasma density or its temperature. When we apply the correction factor of Fig. VI-2 (upper curve) to the peak of the forbidden line, however, the disagreement is effectively removed. The results are less convincing when we attempt to make a similar correction to the intensity midway between the allowed and forbidden lines, by using the lower graph of Fig. VI-2. It may well be that the poorer agreement at this wavelength position results from the fact that the impact approximation for ions is less satisfactory here than it is at the center of the forbidden line.

In conclusion, we see that ion dynamics seems to explain the main differences between experiment and the conventional theory used in calculating Stark-broadened forbidden lines. A final test awaits a more comprehensive theory. Until then, the combined profile of allowed and forbidden lines can be safely used for plasma density determinations, provided only that the results given are appropriately augmented by the correction factors of Fig. VI-2.

B. Ya'akobi, E. V. George, G. Bekefi, R. J. Hawryluk

(Dr. B. Ya'akobi is a member of the Department of Physics and Astronomy, University of Maryland.)

References

1. H. R. Griem, Astrophys. J. 154, 1111 (1968).
2. A. J. Barnard and J. Cooper, J. Quant. Spectrosc. Radiat. Transfer 10, 695 (1970).
3. A. J. Barnard, J. Cooper, and L. J. Shamey, Astron. Astrophys. 1, 28 (1969).
4. D. D. Burgess and C. J. Cairns, J. Phys. B (Atomic and Molec. Phys.) 3, L67 (1970); also see D. D. Burgess, ibid; p. L70.

5. J. W. Birkeland, M. E. Bacon, and W. G. Braun, Phys. Rev. 3, A354 (1971).

6. H. R. Griem, Private communication, 1971.

7. H. R. Griem, Astrophys. J., op. cit. The second term in Eq. (16) of this paper should read $2\Delta\omega_2\Delta\omega_3 C_{22}^2 C_{32}^2(1-R)$.

8. C. F. Hooper, Jr., Phys. Rev. 165, 215 (1968).

9. M. Baranger, in D. R. Bates (Ed.), Atomic and Molecular Processes (Academic Press, Inc., New York, 1962), Chap. 13.

10. H. R. Griem, M. Baranger, A. C. Kolb, and G. Oertel, Phys. Rev. 125, 177 (1962).

11. A. J. Beaulieu, Appl. Phys. Letters 16, 504 (1970); also E. V. George and L. D. Pleasance, Quarterly Progress Report No. 98, Research Laboratory of Electronics, M.I.T., July 15, 1970, p. 47.

12. E. V. George, G. Bekefi, and B. Ya'akobi (a paper submitted to Phys. Fluids).

13. H. R. Griem, Plasma Spectroscopy (McGraw-Hill Book Company, Inc., New York, 1964), see Table 4-4, p. 453.

14. R. Mewe, Brit. J. Appl. Phys. 18, 107 (1967); also H. R. Griem, Plasma Spectroscopy, op. cit., p. 274.

15. W. L. Wiese, in R. H. Huddlestone and S. L. Leonard (Eds.), Plasma Diagnostic Techniques (Academic Press, Inc., New York, 1965), p. 265.

VI. PLASMAS AND CONTROLLED NUCLEAR FUSION*

E. Feedback Stabilization

Academic and Research Staff

Prof. R. R. Parker
Prof. K. I. Thomassen

Graduate Students

R. S. Lowder
A. R. Millner

1. NONLINEAR FEEDBACK CONTROL FOR ALCATOR

Strategy

The successful operation of plasma devices for fusion power will depend upon the production of high-temperature plasmas in a confined volume. A major limitation on the heating currents in Tokamak-type devices is the problem of MHD kink modes of the system, which become unstable at certain threshold current values, with a resulting loss of plasma and energy.

One possible solution to the problem is feedback stabilization of the system. Because such a system would require very large feedback currents and bandwidths, it is most practical to use nonlinear feedback in the form of switches rather than linear amplifiers.

We therefore envision a Tokamak device, enclosed in a conducting shell, with feedback current straps projecting into the vacuum region between the plasma and the shell. A sensing signal is generated for each strap which is a weighted average of the local displacement of the plasma surface. This signal is operated on in some nonlinear fashion, feedback currents flow in the strap, and the result is an additional force on the plasma surface. This force is distributed locally according to a second weighting function. Clearly, with a finite number of sensor outputs, the state of the entire system is not known. Thus much of optimal control theory is not applicable here.

We must now answer certain questions before designing our feedback system. How will feedback affect the stability of the equilibrium? How much current will be needed? How fast must these currents be switched? How many straps are needed, and what is the best geometry for sensing and forcing?

Once these questions have been answered, more pointed conclusions about feasibility, hardware, and experimental questions can be drawn. To approach these

*This work was supported by the U.S. Atomic Energy Commission (Contract AT(30-1)-3980).

questions, we shall first extend the energy principle for hydromagnetic stability to systems with nonlinear feedback. We shall then develop a general description of switched, or "bang-bang" feedback, with stability criteria and design considerations. Then we shall apply our results to a proposal for feedback stabilization of the M.I.T. Alcator device, a high-field Tokamak now under construction.

Notation

Perturbations of the plasma are denoted $\xi(\bar{r}, t)$, where $\bar{r}$ is the position in terms of a periodic cylindrical model, with coordinates $0 < r < a$, $0 < \theta < 2\pi$, and $0 < Z < 2\pi R$. Here a and R are the minor and major radii of the torus. Equilibrium mass density ρ, current $J_Z(r)$, toroidal field H_Z, and poloidal field $H_\theta(r)$ are assumed, with $\bar{H}_o(\bar{r}) = H_\theta(r)\,\hat{\theta} + H_Z\hat{Z}$.

The sensor distribution for the K^{th} feedback strap is denoted $A_K(\bar{r})$, and the resulting signal referred to as the discriminant $D_K(t)$. Our feedback can interact only with the surface of the plasma, which encloses the equilibrium volume V_i. The vacuum region is denoted V_o. A feedback field $\bar{H}_F$ from the K^{th} feedback strap produces a normal force distribution $B_K(\bar{r})$ on S, and the nonlinear signal processing is denoted by the function $F_K(D_K)$.

The proof of self-adjointness of perfectly conducting hydromagnetic systems, which is the basis of the energy principle described by Bernstein et al.[1] and explained in detail by Chandrasekhar,[2] implies the existence of orthonormal modes of such systems. Therefore we write

$$\bar{\xi}(\bar{r}, t) = \sum_m a_m(t)\, \bar{\xi}_m(\bar{r}), \tag{1}$$

modes that are orthogonal in the sense that

$$\int_{V_i} \rho \xi_m \cdot \xi_n \, d\tau = \sigma_{mn}\rho_m. \tag{2}$$

Any convenient normalization may be assumed.

Here we denote by ρ_m the effective mass of the m^{th} mode. Without feedback, the modes behave as $a_m(t) = a_m(0) \cos \omega_m t + a_m(0) \sin \omega_m t/\omega_m$. Therefore we have a positional feedback force normal to S produced by each of N feedback stations, producing a total force

$$\bar{F}_p(\bar{r}, t) = \sum_{K=1}^{N} -B_K(\bar{r})\, \hat{n} F_K(D_K(t)) \tag{3}$$

with discriminant

$$D_K(t) = \int_S A_K(\bar{r})\, \bar{\xi}(\bar{r}, t) \cdot \hat{n}\, dS = \sum_m A_{Km} a_m(t), \tag{4}$$

where we have defined

$$A_{Km} = \int_S A_K(\bar{r})\, \bar{\xi}_m(\bar{r}) \cdot \hat{n}\, dS.$$

The system is diagrammed in Fig. VI-7.

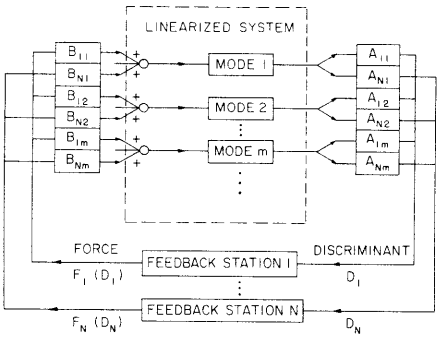

Fig. VI-7. Nonlinear feedback to a linearized distributed system.

If velocity feedback is also desired on S_1 it is assumed to be an additional force of the form

$$F_V(r, t) = \sum_{k=1}^{N} - B'_K(\bar{r})\, \hat{n} F'_K\left(\frac{dD'_K(t)}{dt}\right),$$

with D'_K defined analogously in terms of $A'_K(r)$ and $\xi(r, t)$.

Extension of the Energy Principle

Derivation of the energy principle is rather lengthy and will not be repeated here. Instead, we shall describe the derivation of the equation governing the behavior of each mode amplitude in the presence of externally applied forces. Viscous effects are added later.

The MHD equations of the linearized system can be used to eliminate all variables except the displacement, thereby resulting in the form

$$\rho \frac{\partial^2 \bar{\xi}}{\partial^2 t} = \bar{F}(\bar{\xi}), \tag{5}$$

where $\overline{F}(\overline{\xi})$ is the appropriate linear operator. We dot-multiply (5) with $\overline{\xi}_m(\overline{r})$ to pick out a single mode, and integrate over V_i. Integration of the right-hand side involves use of force equilibrium on the plasma boundary, including the feedback terms. Thus the result is

$$\rho_m\left[\frac{\partial^2 a_m}{\partial t^2} + \omega_m^2 a_m\right] = \int_S \overline{\xi}_m \cdot (\overline{F}_p + \overline{F}_V)\, dS. \tag{6}$$

We may then multiply each mode equation by da_m/dt and sum over all modes to obtain

$$\frac{dE}{dt} = -B, \quad E = T + \Psi + U, \tag{7}$$

where

$$T = \int_V \frac{1}{2}\rho\left|\frac{\partial\overline{\xi}}{dt}\right|^2 d\tau = \sum_m \frac{1}{2}\rho_m\left|\frac{da_m}{dt}\right|^2 > 0$$

$$\Psi = \sum_m \frac{1}{2}\rho_m\omega_m^2 a_m^2 \qquad \left(\omega_m^2 \text{ defined with no viscosity}\right)$$

$$U = \sum_{K=1}^{N}\int_0^{E_k} F_K(D_K)\, dD_k', \qquad E_K = \int_s B_K(\overline{r})\,\overline{\xi}\cdot\hat{n}\, dS$$

$$B = \sum_{K=1}^{N}\dot{E}_K' F_K'(\dot{D}_K') - \sum_{K=1}^{N}\dot{E}_K[F_K(D_K) - F_K(E_K)] + B_V.$$

Here the last term, B_V, represents any viscous effects in the system, with $B_V \geq 0$. The first term in B is due to velocity feedback and has the same damping effect as viscosity. Thus, to avoid pumping energy into the system, we want to design our sensors and enforcers so that $E_K'(\overline{r}) = D_K'(\overline{r})$. Similarly, looking at the second term in B we want $E_K(\overline{r}) = D_K(\overline{r})$. This tells us that the spatial weighting of the sensing and associated forcing elements should be as similar as possible: $A_K(\overline{r}) = B_K(\overline{r})$. Then we require that our feedback functions be restricted to the first and third quadrants, so

$$\int_0^{D_K} F_K(x)\, dx > 0 \tag{8}$$

and $\dot{D}_K' F_K'(\dot{D}_K') > 0$ for all feedback functions F_K.

Bang-Bang Feedback

We now specialize to bang-bang feedback, where F_K is constant in magnitude and changes sign, according to

$$F_K(D_K) = F_K \frac{D_K}{|D_K|} \tag{9}$$

$$F'_K(\dot{D}'_K) = F'_K \frac{\dot{D}'_K}{|\dot{D}'_K|}.$$

Thus, from (7), we now have,

$$U = \sum_{K=1}^{N} F_K |D_K| = \sum_{K=1}^{N} F_K \left| \sum_m A_{Km} a_m \right| \tag{10}$$

$$B = \sum_{K=1}^{N} F'_K |\dot{D}'_K| + B_V.$$

This form of nonlinear feedback has several advantages. It is much easier to implement at high power and bandwidth than linear feedback, and it dominates the dynamics of the system for small perturbations, as can be seen from (7) and (10).

Stability

We then ask, given a system with its modes and growth rates known, how many feedback stations are needed, and how should they be designed for most efficient stabilization?

To answer these questions, we order the modes by ascending algebraic order of ω_m^2. Let M be the (finite) number of modes with nonpositive values of ω^2. We use Lyapunov stability theory, with the state of the system described by the mode amplitudes $a_m(t)$ and velocities $\dot{a}_m(t)$. The norm of the state is defined as $\left[\sum_m \dot{a}_m^2 + \dot{a}_m^2\right]^{1/2} = |\bar{S}|$. We look for a region of stability in this space, such that if the state of the system lies inside this region at sometime t = 0, then its norm will be bounded for all time. This will be true if we can show that for all $\bar{S}$ in the region of stability, where $\bar{S}$ is the state vector,

$$\frac{dE}{dt} \leq 0$$

and

$$\nabla\bar{E} \cdot \bar{S} = \sum \frac{\partial E}{\partial a_m} a_m + \frac{\partial E}{\partial \dot{a}_m} \dot{a}_m > 0 \text{ near } \bar{S} = \bar{0}.$$

This will make E a Lyapunov function of the system in that region bounded by $E(\bar{S}) = E_o = E(\bar{S}_o)$, $\nabla_s E = 0$ at $\bar{S} = \bar{S}_o$.

The first condition is clearly true from (7) and (10) for any $\bar{S}$. We might use velocity feedback to insure its being satisfied for small mode velocities if nonideal effects such as time lag in the feedback system lead to negative terms in B.

The second condition will be satisfied for sufficiently small $|\bar{S}|$ (stability of the null) if we can guarantee that

$$\sum_m \frac{\partial E}{\partial a_m} \cdot a_m = \sum_m \omega_m^2 a_m^2 = 2\Psi > 0$$

for all $\bar{S}$ such that the feedback is unexcited; that is, U = 0, or $D_K = 0$ for all K. Note that if there were no feedback the condition above simply says that all modes of the system must be stable, and so agrees with the energy principle.

To test for null stability, given a feedback configuration, we use $D_K = 0$ to solve for the a_m, $m \leq N$ in terms of the other mode amplitudes. Then we substitute in Ψ and use Sylvester's test for positive definitives of the quadratic form. This test will require only a few calculations in most cases, although the full matrix is infinite dimensional. Further manipulation of this form shows that N = M is the minimum number of feedback stations needed. For instance, by letting each station pick out one mode, N = M is clearly sufficient for that design. We also learn that the design criterion for efficient stabilization is that our feedback have maximum coupling to the first N modes, with minimum coupling to all others. We also require that the separate feedback stations be linearly independent in their spatial distributions. More rigorous treatment shows that we wish to maximize

$$\det \bar{\bar{A}}, \text{ where } A_{ij} = A_{K_m}, \qquad 1 \leq K \leq N, \; 1 \leq m \leq N \tag{11}$$

and $N \geq M$. If practical considerations restrict the design so that the quadratic form Ψ is not positive definite, so that the null is not stable, then it can be stabilized either by improving the design of $A_K(\bar{r})$ or by increasing the number of stations beyond M. Note that, if two unstable modes have exactly the same spatial variation on the surface, $\det \bar{\bar{A}} = 0$, and there is no way to stabilize the system with surface feedback alone. Thus if such modes exist and cause serious disturbance to the system, volume

feedback is required. Generalization of these results to feedback distributed through the volume is not difficult, but physical realization might well be.

Velocity feedback alone can never stabilize an unstable system. Velocity feedback augments viscous effects, however, in minimizing the errors of small time delays and hysteresis in the feedback loops. These effects can be expressed as a negative contribution to B, and are nonzero only for small values of the discriminant. Thus, for any feedback scheme to work, its time delays must be a small fraction of a typical time constant of the system.

Region of Stability

How large a disturbance can be stabilized with this feedback scheme? The answer is best expressed as a region in the state space, such that if the system is initially at any point in the region it will have bounded response for all time. This region is enclosed by some surface. We look for a surface $E(\bar{S}) = \bar{E}_o$, enclosing the origin, such that any initial state within this surface is within the stable region. The value of E_o is found by $\nabla_s \bar{E} = 0$ or $\frac{\partial E}{\partial a_m} = \frac{\partial E}{\partial \dot{a}_m} = 0$ to get

$$\dot{a}_m = 0, \quad a_m^o = -\sum_{K=1}^{N} \frac{F_K A_{Km}}{\rho_m W_m^2} \frac{D_K^o}{|D_K^\circ|}. \tag{12}$$

Solution of these equations involves finding a self-consistent set of a_m° and $D_K^\circ/|D_K^\circ|$, but that is not too difficult, since N is generally small, and so the number of possibilities for the sign of D_K° is manageable. No solution implies global stability of the system.

The region of stability is then bounded by the surface $E(\bar{s}) = E_o$, where

$$E_o = -\sum_m \frac{1}{2\rho_m \omega_m^2} \left[\sum_{K-1}^{N} F_K A_{Km} \frac{D_K^\circ}{|D_K^\circ|} \right]^2 \tag{13}$$

which converges quickly for well-designed systems. Thus, given information about the expected amplitude of disturbances, the required feedback force F_K can be calculated.

One other possible variation should be noted. If the system can be taken as incompressible, and if feedback stations cover the entire surface S, then it is possible to design the system so that it only exerts force in one direction:

$$F_K(D_K) = \frac{F_K}{2} \left(1 + \frac{D_K}{|D_K|} \right). \tag{14}$$

The result is that the first term in (14) has no net effect, and so the effective bang-bang force is half that which is applied.

Alcator

The proposed Tokamak-type device now under construction at M.I.T. is a possible application of the above-mentioned feedback scheme. It is a toroidal device, with the following approximate projected operating range[3]:

Major radius $R = 0.5$ m

Minor radius of plasma $a = 0.13$ m of shell $R_W = 0.15$ m

Toroidal field $H_Z = 130$ kG $\hat{=} 10^7$ A/m

Particle density $N_o = 5 \times 10^{20}/m^3$

Mass density $\rho = 8 \times 10^{-7}$ kG/m^3 (protons)

Estimated $q = \frac{H_Z a}{H_\theta(a) R} \geq q_o = 2.5$ without feedback,

where (r, θ, Z) are consistent with a periodic cylinder model.

The purpose of putting feedback on such a device would be to alter the dynamics so as to lower the value of q consistent with stability of the surface. As long as there is a vacuum region between the conducting shell and the plasma, $q >$ some q_o will be a limitation on the heating current. Ideally, feedback would allow any value of heating current without instability of the surface.

We have a modelling problem in designing this system. Theoretical predictions of growth rates are unreliable and depend critically upon the radial current distribution, which is difficult to measure. Therefore we shall choose a simple uniform current distribution ($J_Z(\bar{r})$ = constant), and assume these results to be approximately correct for real situations. We take our modes to be expressed as a Fourier transform of the normal surface perturbation and let the radial variation adapt itself to satisfy the equations of the system. Thus on S,

$$\xi_r(\bar{r}) = \sum_{i=0}^{1} \sum_{j} \sum_{m=0}^{\infty} \sum_{n=-\infty}^{\infty} a_{ijmn}(t) \cos\left(m\theta + \frac{nZ}{R} + i\frac{\pi}{2}\right),$$

where we have normalized $\bar{\xi}_{ijmn}(\bar{r})$ so that the maximum value of ξ_r on S is unity. We expect the worst situations to occur when the $m = n = 1$ mode approaches the interchange condition. Therefore our operating point will be assumed to lie near $q \hat{=} -1$ or $H_\theta(a) \hat{=} -H_Z \frac{a}{R} = -2.5 \times 10^6$ A/m.

Design

We refer to the work of Shafranov[4] and others for derivation of the dispersion relation and final form of the modes. For convenience, we define the following quantities:

$\phi = m + nq$ (a measure of deviation from interchange condition)

$$Y_{mn}^2 = -\rho \frac{\omega_{imn}^2 a^2}{\mu_o H_\theta^2(a)} \quad \text{(growth rate)}$$

For long-wavelength modes ($na/R \ll 1$) the following dispersion relation applies:

$$Y_{mn}^2 = \frac{1}{2}\left[\phi - \frac{\phi^2}{1 - \left(\frac{a}{R_W}\right)^{2m}}\right]. \tag{15}$$

This gives a maximum growth rate of

$$Y^2 = \frac{1}{2}\left[1 - \left(\frac{a}{R_W}\right)^{2m}\right] \quad \text{when} \quad \phi = \frac{1}{2}\left[1 - \left(\frac{a}{R_W}\right)^{2m}\right]. \tag{16}$$

Inserting Alcator parameters, this gives $Y^2 = \phi \stackrel{\circ}{=} 0.13$. Taking $m = n = 1$, we see that $q \stackrel{\circ}{=} -0.87$ is in the expected range. Higher m modes would be unstable at higher q but experience has shown them to be less of a problem in terms of confinement. The growth rate, then, is given by

$$-\omega_{ill}^2 = 7 \times 10^{13}\ s^{-2}$$

$$|\omega_{ill}| \stackrel{\circ}{=} 8 \times 10^6\ s^{-1}.$$

The time $\tau = 1/\omega \stackrel{\circ}{=} 1.2 \times 10^{-7}$ s represents the maximum time scale that we can afford to allow in feedback time lag, because of switching, processing, and so forth.

In addition to these modes, there may be others (j) with the same m and n, but more complex radial dependence. These are all stable, or nearly so. In certain ranges of operation near $q \stackrel{\circ}{=} -1$, however, theory predicts that these modes can combine with the original kink mode to produce an unstable perturbation, with zero surface deflection but unstable internal behavior. We refer to these combinations as internal modes, since they satisfy the equations of the system with a new boundary condition namely, $\xi_r(a) = 0$.

Such internal modes, if unstable, represent a severe limitation on surface-coupled feedback. They represent the limit of the null stability test mentioned above, where only mode amplitudes of the $m = n = 1$ modes need be considered. If they grow without limit, eventually such modes will overwhelm the feedback, and enter a new phase of growth dominated by the fast-growing kink. It is quite possible, however, that mechanisms not included in our model will stabilize such modes before they get out of hand,

since their growth rate is small. This must be verified by experiment.

We shall assume that the long-wavelength modes analyzed first are the only ones present. Then we can use (12) and (13) to calculate the magnitude of feedback needed for expected disturbances to lie within the region of stability.

The first thing we notice is that a_m° becomes very small and makes little contribution to E_o when ω_m^2 becomes large and positive. For $m/n \neq 1$ this is the case, so we can ignore the effect of these modes. Then we note that for high m and n numbers, even if $m/n = 1$ and our model predicts instability, we expect other effects (such as finite Larmour radius) to stabilize such modes. So, for a first approximation, we shall assume that $m = n = 1$ are the only modes that we need consider. If experiment proves this wrong, then modification is clearly possible, but present available results do not contradict this assumption.

We therefore have two unstable modes, from $i = 0$ and $i = 1$. This implies two current straps if we can both push and pull on the plasma, or four if we can only push. The first would be an option if we rely on a forcing term $\overline{H}_o \cdot \overline{H}_f$ on S and reverse the current. The second is possible also from a term H_F^2, which can be significant with bang-bang feedback. All other higher terms can be ignored if $|\overline{H}_F| \ll |\overline{H}_o|$. The first option would appear to require the least current, but, as we shall see, its contribution vanishes at the interchange condition. This aspect will be discussed later. To do so, we use (12) to evaluate the current needed in each scheme to stabilize a kink mode with maximum surface perturbation of $a_m^\circ = \frac{1}{2}(R_W - a) = 10^{-2}$ m.

First, we must calculate the equivalent mass. Since we have $\frac{a}{R} \ll 1$, this gives

$$\rho_m^\circ = \frac{1}{2}[2\pi^2 a^2 R]^\circ = 6 \times 10^{-8} \text{ kG}.$$

We denote the coupling term A_{Km} for $i = 0$ or 1, $n = m = 1$ by A_{K11}. We must now evaluate the coupling coefficients A_{Km} and determine the currents needed. Equation 12 requires that $F_K A_{K11} = 8 \times 10^3$ N.

To simplify the evaluation of $F_K A_{K11}$, we note that

$$\int_S \mu_o \overline{H}_1 \cdot \overline{H}_2 \overline{\xi}_m \cdot \hat{n}\, dS = \int_{V_o} \hat{A}_{1m} \cdot J_2\, d\tau, \tag{18}$$

where $J_2 = \nabla \times \overline{H}_2$ in the vacuum region V_o, and $\hat{A}_{1m}$ is the vector potential in that region, because of the perturbation of H_1 by $\overline{\xi}_m$. It satisfies the boundary condition on S, the plasma surface, that

$$\hat{n} \times \hat{A}_{1m} = -H_1 \mu_o (\overline{\xi}_m \cdot \hat{n}). \tag{19}$$

Thus we may rewrite the effective force as

$$F_K A_{K11} = \frac{1}{2}\int_S \mu_o \overline{H}_o \cdot \overline{H}_F + \frac{1}{2}\mu_o H_F^2 \overline{\xi}_H \cdot \hat{n}\, dS$$

$$= \int_{V_o} \hat{A}_{11} \cdot J_F + \frac{1}{2}\hat{A}_{F11} \cdot J_F \, d\Upsilon, \tag{20}$$

where $\hat{A}_{11}$ represents the perturbation vector potential attributable to $\overline{\xi}_{11}$ without feedback, and $\hat{A}_{F11}$ the perturbation of the feedback field alone. We must then place wires so that current will flow along vector potential lines, and so that the current is determined by the flux linked by the wire.

For velocity feedback, our integral becomes $\overline{E}_{11} \cdot \overline{J}_F$, where $\overline{E}_{11}$ is the electric field $-\frac{\partial A_{11}}{\partial t}$, because of the perturbation, without feedback added. Linear velocity feedback is properly applied by any slightly conducting substance inside the conducting shell, so that its resulting $\partial H_F/\partial t$ creates an electric field much smaller than the perturbation field. Our damping interpretation corresponds to standard energy perturbation results.

We must now estimate the vector potentials $\hat{A}_{11}$ and $\hat{A}_{F11}$ at the feedback wires. Since $R_W - a \ll a$, we may model the vacuum region as a planar geometry. Analysis of $\hat{A}_{11}$, the perturbation vacuum potential, shows that it divides into two parts, one irrotational and one solenoidal. The irrotational part produces an electric field with $E = -\nabla\Phi$, where for any mode m and n,

$$\Phi(r, o, z) = \mu_o \omega_{mn} \frac{\left(\frac{n}{R} H_\theta(a) - \frac{m}{a} H_z\right) \sinh K(r-R_W)\, \xi_{rmn}(a)}{K^2 \sinh K(R_W-a)},$$

where

$$K^2 = \left(\frac{n}{R}\right)^2 + \left(\frac{m}{a}\right)^2.$$

Coupling to this field would have to be electric, and so is relatively small for realistic feedback fields.

The solenoidal part produces the perturbation magnetic field. This vector potential is given by

$$A_{11}(r, \theta, z) = \frac{\mu_o\left(\frac{n\theta}{R} - \frac{mz}{a}\right)(m+nq)\, H_\theta(a) \sinh K(r-R_W)\, \xi_{rmn}(a)}{K^2 a \sinh K(R_W-a)}. \tag{21}$$

This is the term to which we can couple.

We should notice several things about the potential. First, it points along flutes of the surface perturbation and parallel to the equilibrium surface. Thus, this is the direction in which our feedback currents should go, as far from R_W as possible, to maximize the term $\bar{H}_o \cdot \bar{H}_F$ (see Fig. VI-8). Second, the term vanishes when $m + nq = 0$, so such feedback will not affect the interchange modes. Thus, this term will dominate situations far from the interchange situation.

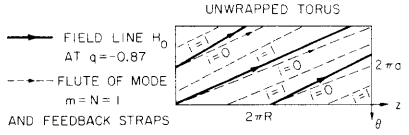

Fig. VI-8. Feedback geometries for Alcator.

Finally, we note that this term is proportional to $\frac{m}{a} H_\theta(a) + \frac{n}{R} H_Z = \bar{K} \cdot \bar{H}_o$ at $r = a$, where we define the wave vector $\bar{K} = \frac{m}{a}\hat{\theta} + \frac{n}{R}\hat{Z}$. This gives us an easy way to evaluate $\hat{A}_{F11}$, the vector potential attributable to the perturbations of the feedback field. We can simply replace the factor with $\bar{K} \cdot \bar{H}_F(a)$. This means that, to maximize the H_F^2 force term, the feedback field should be perpendicular to the flutes, and the feedback currents parallel to them. We therefore see that this geometry is also optimum for feedback contributions of the H_F^2 term. To the extent that $\bar{H}_F(a)$ can be approximated as a constant, this geometry gives

$$\hat{A}_{Fmn} = \frac{\mu_o\left(\frac{n\hat{\theta}}{R} - \frac{m\hat{Z}}{a}\right)(\bar{H}_F(a) \cdot \bar{K}) \sinh K(r-R_W)\, \xi_{rmn}(a)}{K^2 \sinh K(R_W - a)} . \tag{22}$$

If the total current in the strap is limited, then clearly we want it all to flow in a wire sitting at maximum vector potential, to maximize (20). Let us assume that the $\bar{H}_F \cdot \bar{H}_o$ term dominates. The length of wire is approximately $2\pi r$. This gives a current needed of

$$I_{F_1} = \frac{2F_K A_K}{2\pi R|\hat{A}_{11}|} \approx 2 \times 10^4 \text{ A.}$$

Now let us assume that the H_F^2 term dominates. This leads to an estimate

$$I_{F2} \approx \frac{2F_K A_K}{2\pi R \hat{A}_{F11}} \approx 3 \times 10^4 \text{ A.}$$

The two are quite close. In fact, the value of q at which we assumed we were

operating is close to the "break point" between the two extremes. As $q \to -1$, the nonlinear term dominates.

When designing the feedback straps, a major consideration will be to minimize the inductance, to avoid arcing during switching transients. This involves maximizing (20) while minimizing the integral over V_o of $\frac{1}{2}\mu_o H_F^2$. We can see that a single wire, or impulse of current, would cause very large local magnetic field energy and so is not a good choice. To explore the modification, we assume $\overline{K}_F$ to be distributed in a plane parallel to the equilibrium plasma surface. Its Fourier components produce corresponding components of magnetic field and, since they are orthogonal over the vacuum region, their energies add. Thus, to minimize inductance, we want to distribute the current sinusoidally to match the vector potential and surface perturbation. This is just the distribution of current that occurs on the conducting sheath, a form of linear feedback. Thus the effect of the $\overline{H}_F \cdot \overline{H}_o$ type of feedback is to make the conducting sheath appear arbitrarily close to the plasma, as increasing the gain of a linear feedback system, if such were contemplated. Its maximum effect is that of a wall as $R_W \to a$, and this is the effect of bang-bang on the modes $m = n = 1$.

Note that the use of H_F^2 feedback lets us do even better, by stabilizing interchange modes that are unaffected by a wall arbitrarily close to the plasma.

We also note that the spreading of feedback currents over a sinusoid results in a decrease in effectiveness because not all the current is at maximum $\hat{A}$. This will roughly cancel the addition of terms in our calculation of current, if the current in a strap is equated to the positive half-cycle of a sinusoid. The resulting inductance for such a scheme is approximately 1.3×10^{-7} H. Assuming the rise time of $1.2 < 10^{-7}$ s, this gives voltages of 33 kV during switching; difficult but not impossible to work with.

Thus, we would design our feedback so that the currents flow just above flutes in the surface ($\overline{J}_F \times \overline{H}_o \cdot \hat{r} > 0$). For 1-cm perturbations, we require that approximately 30,000 A be switched in less than a tenth of a microsecond. This would be difficult, but not impossible. Certainly at these currents, linear feedback would be far more difficult. Our experiment would look for increased confinement time, and check assumptions that modes with fast spatial variations will be damped.

In conclusion, we can see that the analysis of nonlinear feedback to continuous systems is quite workable. It applies to some very important physical situations, and can be used with various degrees of approximation. In application to Alcator, it appears feasible to use bang-bang feedback in order to allow lower values of q, while preserving finite separation between plasma and conducting shell. The region of q-operation desired will determine the feedback mode of operation.

The authors are grateful to Prof. James R. Melcher of the Department of Electrical Engineering, M.I.T., for his advice and assistance in this work.

A. R. Millner, R. R. Parker

References

1. I. B. Bernstein, E. A. Frieman, M. D. Kruskal, and R. M. Kolsrud, "An Energy Principle for Hydromagnetic Stability Problems," Proc. Roy. Soc. (London) A 244, 17-40 (1958).
2. S. Chandrasekhar, Hydrodynamic and Hydromagnetic Stability (Clarendon Press, Oxford, 1961), Chap. 14, "A General Variational Principle."
3. B. Coppi and B. D. Montgomery, Proposal to the U.S. Atomic Energy Commission for a High Magnetic Field Toroidal Experiment ALCATOR for the Investigation of High Temperature Plasmas, October 1969.
4. V. D. Shafranov, "Hydromagnetic Stability of a Current-Carrying Plasma Column in a Strong Longitudinal Magnetic Field," Kurchatov Report IAE-1853, Moscow, May 1969, pp. 1-28.
5. J. R. Melcher, "Feedback Stabilization of Hydromagnetic Continua; Review and Prospects: Feedback and Dynamic Control of Plasmas," A.I.P. 1970, pp. 38-53.

2. ON THE REQUIREMENTS FOR FEEDBACK STABILIZATION OF KINK MODES IN A CURRENT-CARRYING PLASMA

Introduction

In the last quarterly progress report[1] a guiding center model of the kink instability in a uniform current plasma cylinder was presented. By using this model, a stability criterion was obtained which included the effects of external feedback currents. In this report we shall consider a plasma in which the current is concentrated in a thin sheet at the plasma vacuum boundary.

A stability criterion is derived by extending the analysis of a sheet pinch in a strong longitudinal magnetic field presented by Kadomtsev[2] to include external feedback currents. We shall show that the feedback requirements for the m = 1 mode are the same for both the uniform and thin-sheet current distributions.

Sheet Pinch

The cylindrical column, radius a, is immersed in a strong axial field B_z and separated from the feedback currents at r = b by a vacuum region. The surface current at r = a produces the field

$$B_\theta = \begin{cases} 0 & r < a \\ B_a \frac{a}{r} & r > a \end{cases} \tag{1}$$

The field B_z is uniform throughout the vacuum and plasma regions and is much larger than B_a.

To examine the stability of this configuration, we make a perturbation $\bar{\xi}$,

whose radial component at the boundary is

$$\xi_r\Big|_{r=a} = \xi_{a_o} \exp(im\theta - ik_z z + \gamma t) = \xi_a. \tag{2}$$

The perturbed vacuum magnetic field is $\tilde{B} = \nabla\psi$, with $\nabla^2\psi = 0$. Solving the ideal MHD equations and equating total pressure across the perturbed boundary determines ξ_a. Following Kadomtsev,[2] we find for $k_z a \ll 1$ and an incompressible plasma

$$\left[\rho\mu_o\gamma^2 + k_z^2 B_z^2\right]\xi_a^2 = -\frac{m}{a}\left[\frac{\psi_a\psi_a'}{\xi_a} - B_a^2\frac{\xi_a}{a}\right]\xi_a, \tag{3}$$

where ρ is the mass density (assumed constant), $\psi' = \frac{\partial\psi}{\partial r} = \tilde{B}_r$, and $\psi_a = \psi(r=a)$. The left side of Eq. 3 is the internal gain of kinetic plus magnetic energy, and the right side is the displacement times the pressure gradient owing to the perturbed magnetic field. We require continuity of pressure across the perturbed boundary, which determines the pressure gradient there and brings in the $\psi_a\psi_a'$ term on the right-hand side of Eq. 3. We can now modify $\psi_a\psi_a'$ to include the feedback currents.

The magnetic potential (for $k_z a \ll 1$) is approximately

$$\psi \approx C_1\left(\frac{a}{r}\right)^m + C_2\left(\frac{r}{b}\right)^m,$$

where C_1 and C_2 are determined by boundary conditions. At $r = a$, $\bar{B}\cdot\nabla\phi = 0$, where $\phi(r,\theta,z) = r - a - \xi_r = 0$ is the perturbed surface. Since $\nabla\phi = \left(1, -\frac{im\xi_a}{r}, +ik_z\xi_a\right)$, the "field freezing" condition ($\bar{B}\cdot\nabla\phi = 0$) is

$$\psi_a' = \tilde{B}_r(r=a) = i\frac{m}{a}B_\theta(a)\,\xi_a - ik_z B_z(a)\,\xi_a = ik_{\|}B\xi_a, \tag{4}$$

where $k_{\|} \equiv (mB_a/a - k_z B_z)/B$.

At $r = b$, ψ' is continuous but the tangential field has a jump $\mu_o K_f$, where K_f is the feedback current and is of the form

$$K_f = K_{fo}\, e^{im\theta - ik_z z + \gamma t}$$

These two boundary conditions determine C_1 and C_2:

$$\frac{-im\,C_2}{b} = \frac{\mu_o K_f}{2}$$

and

$$\frac{-im\,C_1}{b} = \frac{\mu_o K_f}{2}\left(\frac{a}{b}\right)^m - k_{||}B\xi_a\frac{a}{b}.$$

If we take a feedback current proportional to the boundary displacement, but opposed to the direction of zero-order current, namely

$$K_f = -G\xi_a \quad \text{or} \quad G = -K_{fo}/\xi_{a_o} \text{ (units of } A/m^2), \tag{5}$$

we find that Eq. 4 becomes

$$\psi = -\frac{ib}{m}\frac{\mu_o G\xi_a}{2}\left[\left(\frac{a}{b}\right)^m\left(\frac{a}{r}\right)^m + \left(\frac{r}{b}\right)^m\right] - \frac{ia}{m}k_{||}\xi_a B\left(\frac{a}{r}\right)^m. \tag{6}$$

Using Eq. 6, we can compute the pressure gradient terms in Eq. 3. First,

$$\frac{m}{a}\frac{\psi_a\psi'_a}{a} = (k_{||}B)^2\xi_a + k_{||}B\mu_o G\left(\frac{a}{b}\right)^{m-1}\xi_a,$$

so that Eq. 3 becomes

$$\rho\mu_o\gamma^2 + (k_z B_z)^2 + (k_{||}B)^2 - \frac{mB_a^2}{a^2} = -k_{||}B\mu_o G\left(\frac{a}{b}\right)^{m-1}. \tag{7}$$

Stability requires $\gamma^2 < 0$, or

$$\mu_o G k_{||}B\left(\frac{a}{b}\right)^{m-1} > \frac{mB_a^2}{a^2} - (k_z B_z)^2 - \left(\frac{m}{a}B_a - k_z B_z\right)^2.$$

If we define $q = aB_z/RB_a$ and $k_z = n/R$ (with toroidal geometry in mind) the criterion can be written

$$(m-nq)\frac{\mu_o G}{2}\left(\frac{a}{b}\right)^{m-1} > k_z B_z\left[1 - \frac{m-1}{nq}\,\frac{m}{2(m-nq)}\right](m-nq). \tag{8}$$

The corresponding result for the uniform current distribution is[1]

$$(m-nq)\frac{\mu_o G}{2}\left(\frac{a}{b}\right)^{m-1} \geq k_z B_z\left[1 - \frac{m-1}{nq}\right](m-nq). \tag{9}$$

To determine the stabilizing influence of a wall at r = b, rather than feedback currents, we choose the value of G which makes $\tilde{B}_r|_{r=b} = 0$ in order to simulate a conducting wall. From Eq. 6, $\psi'_b = 0$ if

$$\frac{\mu_o G}{2} = k_{||} B \frac{(a/b)^{m+1}}{1 - (a/b)^{2m}}.$$

Substituting this value of G in Eq. 7 gives the correct wall stabilized growth rate[3-5]

$$\rho\mu_o\gamma^2 + (k_z B_z)^2 - \frac{mB_a^2}{a^2} = (k_{||}B)^2 \frac{1 + (a/b)^{2m}}{1 - (a/b)^{2m}}. \tag{10}$$

Discussion

We have derived the required gains to stabilize both the uniform and thin-sheet current distributions. An interesting comparison can be made in terms of the vacuum field B_f produced by the feedback coils in the absence of a plasma. Since the feedback current is $K_f = -G\xi_a$, we find

$$|\overline{B}_f(r=a)| \equiv B_{fa} = \frac{\mu_o}{2}\left(G\xi_{a_o}\right)\left(\frac{a}{b}\right)^{m-1}.$$

In terms of this field, the feedback requirements are the following.

1. Uniform or thin-sheet current, m = 1 (mode unstable with q < 1 without feedback)

$$B_{fa} \geq \left(k_z \xi_{a_o}\right) B_z.$$

2. Uniform current m ≥ 2 (mode unstable with m - 1 < nq < m without feedback)

$$B_{fa} \geq \left(k_z \xi_{a_o}\right) B_z \left(1 - \frac{m-1}{nq}\right).$$

For the sheet currents, m ≥ 2 modes are stable (all q) without feedback.

From this comparison between the uniform and thin-sheet currents we see that the criteria for stabilization of the higher order modes are dependent on the current distribution and on q. Criteria for feedback stabilization of the m = 1 mode, however, are the same for these two distributions and independent of q (depending only on B_z and k_z which is fixed in toroidal geometry). Shafranov[6] has stated that the growth rate for the m = 1 mode is independent of current distribution. Hence we speculate that the feedback requirements too are independent of current distribution for the m = 1 mode.

R. S. Lowder, K. I. Thomassen

References

1. R. S. Lowder and K. I. Thomassen, Quarterly Progress Report No. 101, Research Laboratory of Electronics, M.I.T., April 15, 1971, pp. 81-87.
2. B. B. Kadomtsev, Reviews of Plasma Physics, Vol. 2, Consultants Bureau 1966, See Equations 7.3 and 7.5.
3. R. J. Taylor, Proc. Phys. Soc. (London) 70B, 31 (1957).
4. V. D. Shafranov, Plasma Physics and the Problem of Controlled Thermonuclear Reactions (Pergamon Press, London, 1959), Vol. 2, p. 197 and Vol. 4, p. 171.
5. M. D. Kruskal and J. L. Tuck, Proc. Roy. Soc. (London) A245, 222 (1958).
6. V. D. Shafranov, Soviet Phys. - Tech. Phys. 15, 175 (1970).

VI. PLASMAS AND CONTROLLED NUCLEAR FUSION*

F. High-Temperature Toroidal Plasmas

Academic and Research Staff

Prof. B. Coppi
Dr. D. B. Montgomery†
Prof. G. Bekefi
Prof. A. Bers
Prof. R. A. Blanken
Prof. R. J. Briggs
Prof. L. M. Lidsky
Prof. R. R. Parker
Prof. K. I. Thomassen
Dr. U. Daybelge
Dr. R. Gajewski
Dr. P. A. Politzer
Dr. D. J. Sigmar

Graduate Students

E. L. Bernstein
R. Dagazian
D. P. Hutchinson
Y. Y. Lau
M. A. Lecomte
A. R. Milner
M. Simonutti
E. N. Spithas
B. V. Waddell
D. C. Watson

1. ALCATOR LOWER HYBRID-HEATING EXPERIMENT

Introduction

A unique feature of the M.I.T. Alcator experiment will be the application of a high-power, S-band beam whose primary purpose will be to heat the plasma to temperatures significantly higher than those attainable by ohmic heating. In addition to providing additional energy input, this experiment will give rise to related experiments that will be of great interest. For example, by modulating microwaves it may be possible to couple to low-frequency modes, thereby changing the population level of trapped particles. Also, by pulsing the radio frequency and observing the resulting energy rise and decay times, it should be possible to make simple and direct measurement of these important times. Finally, the presence of RF should enhance the classical plasma resistivity, thereby increasing energy absorption from the confining current.

A scheme for plasma heating at the lower hybrid frequency was described several years ago by Stix.[1,2] In this scheme RF energy excites a wave at the plasma boundary, which then propagates nearly perpendicularly to the magnetic field. This wave, which rapidly becomes electrostatic, is slowed down still further as it propagates into the vicinity of the lower hybrid resonance.

The ultimate fate of the wave is still the subject of speculation; cold-plasma theory predicts complete absorption, independent of the absorption mechanism. Stix has pointed out that the wave can convert at the hybrid resonance to an ion plasma wave, which might then be absorbed by cyclotron-harmonic damping or, as seems more likely,

*This work was supported by the U.S. Atomic Energy Commission (Contract AT(30-1)-3980).

†Dr. D. Bruce Montgomery is at the Francis Bitter National Magnet Laboratory.

may be directly Landau-damped. There are other possibilities; for example, nonlinear effects may completely dominate any linear absorption mechanism, or the wave may bend and become a propagating mode parallel to the magnetic field. This question is an interesting one for future work.

In this report we discuss some aspects of the proposed heating experiment. We first re-examine the accessibility condition, that is, the criterion for insuring that the wave approaches the resonance from a region of propagation rather than evanescence. This condition was first given by Stix; however, we give a somewhat less stringent condition. We calculate the impedance presented to an electromagnetic structure at the lower hybrid frequency. The density gradient can act as an impedance transformer, with the result that a reasonable impedance is presented to the structure. Finally, the mechanism by which the energy is transported to the resonant layer is investigated. We find that for a gap excitation, the disturbance "propagates" nearly parallel to the magnetic field, at an angle $\sim(m/M)^{1/2}$. This is so because the group velocity is nearly perpendicular to the phase velocity, as it is for any electrostatic cold-plasma mode.

Accessibility Condition

The lower hybrid resonance is a wave resonance (as opposed to a particle resonance) which occurs for a wave propagating essentially perpendicular to the magnetic field. For most laboratory plasmas, the resonant frequency is well below electron cyclotron frequency but well above ion cyclotron frequency. The resonant frequency is, in general, a function of density and magnetic field, but for Alcator parameters occurs nearly at the ion plasma frequency. Thus the heating scheme is to launch a wave at the liner, in the region of low density from whence it propagates to the core of the Alcator plasma where the energy can be absorbed at a point where the local ion-plasma frequency becomes equal to the applied frequency. For the scheme to make sense, it is essential that the wave be propagating, rather than evanescent, from the wall to the resonant layer. This condition has been called by Stix the accessibility condition.

The question of accessibility can be handled appropriately by cold-plasma theory, since, as we shall see, the phase velocity of the wave parallel to the magnetic field is fast; that is, nearly c, while the wavelength perpendicular to the magnetic field is large compared with either the ion or electron Larmor radius, except in the immediate neighborhood of the resonance. Thus we first examine the dispersion equation for waves in a cold plasma. This can be written in the form

$$n_x^4 K_\perp + n_x^2\left[(K_\parallel+K_\perp)\left(n_z^2-K_\perp\right)-K_x^2\right] + K_\parallel\left[\left(n_z^2-K_\perp\right)^2+K_x^2\right] = 0, \tag{1}$$

where n_x^2 and n_z^2 are components of the index of refraction perpendicular and parallel to the magnetic field, respectively, and $K_\perp$, K_x and $K_\parallel$ are the familiar components

of the cold-plasma dielectric tensor. For frequencies well below the electron gyro frequency, ω_{ce}, but well above the ion gyro frequency ω_{ci}, these quantities are given by

$$K_{\perp} \approx 1 - \frac{\omega_{pi}^2}{\omega^2} + \frac{\omega_{pe}^2}{\omega_{ce}^2} \tag{2a}$$

$$K_x \approx j \frac{\omega_{pe}^2}{\omega\omega_{ce}} \tag{2b}$$

$$K_{\parallel} \approx 1 - \frac{\omega_{pe}^2}{\omega^2}, \tag{2c}$$

where ω_{pe}^2 $\left(\omega_{pi}^2\right)$ is the electron (ion) plasma frequency. A wave resonance (infinity in n_x^2) clearly occurs when $K_{\perp} = 0$, or from Eq. 2a, $\omega = \omega_{\ell h}$, with

$$\omega_{\ell h}^2 = \frac{\omega_{pi}^2 \omega_o^2}{\omega_{pi}^2 + \omega_o^2} \tag{3}$$

and

$$\omega_o^2 = \omega_{ce}\omega_{ci}.$$

We note from Eq. 1 that the only other possible wave resonances occur when the elements $K_{\perp}$ and K_x are infinite, that is, the ion and electron gyro frequencies. These resonances, unlike the hybrid resonance, are associated with <u>particle</u> resonances; that is, for finite electric field, the particle RF velocities are infinite. In the present case, large particle velocities occur only because of a resonant electric field. Consequently, nonlinear effects may be important in the ultimate disposition of the wave energy.

For the Alcator plasma we expect

$$\omega_o^2 \approx 10\ \omega_{pi}^2,$$

so the resonant frequency is nearly equal to the ion plasma frequency. At a density of 10^{14} cm^{-3}, this frequency is 2.1 GHz, corresponding to a free-space wavelength of ~15 cm. The fact that the resonant frequency occurs at ω_{pi}^2, rather than ω_o^2, is important.

An elementary calculation shows that the ratio of RF ion energy to RF electron energy in this frequency range is ω_o^2/ω^2. Since $\omega^2 \approx \omega_{pi}^2 \approx 10^{-1}\,\omega_o^2$, the ion RF energy will exceed that of the electrons by approximately an order of magnitude. Thus we hope that a significant fraction of the wave energy will be deposited in the ions. Also, we note that the location of the resonant frequency at an ion-plasma frequency in the microwave region where the free-space wavelength is less than the diameter of the plasma distinguishes the Alcator lower hybrid-heating experiment from all of the lower hybrid work done thus far, in particular that of the Texas group.[3]

Returning to the accessibility question, we note from Eq. 1 that as $K_\perp \to 0$, the resonant root is given by

$$n_x^2 \to -\frac{K_{||} n_z^2 - K_x^2}{K_\perp}. \tag{4}$$

In approaching the lower hybrid resonance through values of density below the critical value, that for which $K_\perp = 0$, we observe that $K_\perp > 0$ while both K_x^2 and $K_{||}$ are negative. So a necessary condition for approaching the resonance from a region of propagation is $n_z^2 > \frac{|K_{x_o}^2|}{K_{||o}}$ where K_{x_o} and $K_{||o}$ are the values of K_x and $K_{||}$ at the critical density. Detailed investigation reveals that this condition is not sufficient, since even if it is satisfied, a region of complex waves, which carry no power, may be encountered between the wall (zero density) and the resonant density.

In order to examine the dependence of n_x^2 or n_z^2 and density, we rewrite the elements of the dielectric tensor in the form

$$\begin{aligned} K_\perp &= 1 - \tilde{n} \\ K_x &= j\sqrt{\beta}\,\tilde{n} \\ K_{||} &= 1 - \alpha\tilde{n}, \end{aligned} \tag{5}$$

where $\tilde{n} = n/n_o$, the ratio of density to critical density, $\beta = \frac{\omega_{pe_o}^2}{\omega_{ce}^2}\,\alpha$ and $\alpha = \frac{M}{m}\left(1 + \frac{\omega_{pe_o}^2}{\omega_{ce}^2}\right)$, where $\omega_{pe_o}^2$ is the electron plasma frequency evaluated at the resonant layer, and M/m is the mass ratio. For Alcator parameters, $\beta \sim 10^{-1}\,\alpha$ and α is essentially the mass ratio.

The solution of Eq. 1 sketched vs $\tilde{n}$ with n_z^2 as a parameter is shown qualitatively

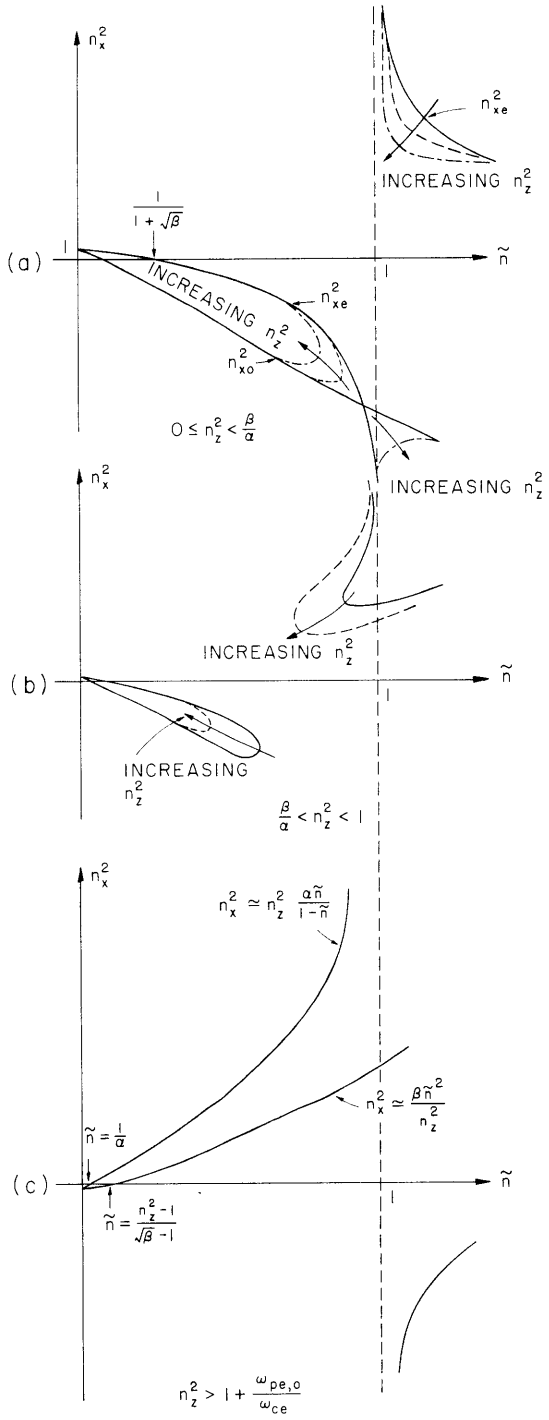

Fig. VI-9. Schematic behavior of n_x^2 vs normalized density with n_z^2 as a parameter: (a) $0 < n_z^2 < \beta/\alpha$; (b) $\beta/\alpha < n_z^2 < 1$; (c) $n_z^2 > 1 + \sqrt{\beta/\alpha}$.

in Fig. VI-9. In Fig. VI-9a the solution is shown first for $n_z^2 = 0$, in which case the dispersion equation factors into the ordinary and extraordinary modes

$$n_{xo}^2 = K_{\parallel} = 1 - \alpha\tilde{n}$$

$$n_{xe}^2 = \frac{K_{\perp}^2 + K_x^2}{K_{\perp}} = 1 - \tilde{n} - \beta\frac{\tilde{n}^2}{1-\tilde{n}}.$$

Since $\sqrt{\beta} \sim 15$, the extraordinary mode is cut off in most of the plasma up to the resonant layer ($\tilde{n}<1$). Consequently, there would be little hope for using this branch to heat the plasma directly. [In fact, the tunneling factor is of the order of

$$e^{-\int_0^{x_o} |k_x|\,dx},$$

where x_o is the position of the resonance. For a linear density profile this factor is $\sim e^{-ax_o}$, where

$$a = k_o\sqrt{\beta}\int_0^1 \frac{x}{\sqrt{1-x}}\,dx = \frac{4k_o\sqrt{\beta}}{3}$$

with $k_o = \omega/c$. If x_o is near the center of the machine, $k_o x_o \sim 2\pi$, and since $\sqrt{\beta} = 15$, the tunneling factor is $\sim e^{-120}$!] As n_z^2 is increased, a coupling between the ordinary and extraordinary modes takes place near the resonance as shown. Finally, at a critical value, $n_z^2 = \frac{\beta}{\alpha}$, the resonance is approached through positive values of n_x^2 for $\tilde{n} < 1$, as predicted by Eq. 4. This behavior is shown schematically in Fig. VI-9b. Note the absence of real n_x^2 solutions for regions of $\tilde{n}$. The solutions here are complex, indicating complex waves that carry no power. Finally, for larger n_z^2, the solution has the appearance shown in Fig. VI-9c. The value of n_z^2 which causes this transition can be found by demanding from Eq. 1 that the solution for n_x^2 be real. This requires

$$\left[(K_{\parallel}+K_{\perp})\left(n_z^2-K_{\perp}\right)-K_x^2\right]^2 - 4K_{\parallel}K_{\perp}\left[\left(n_z^2-K_{\perp}\right)^2+K_x^2\right] > 0.$$

The left-hand side of this inequality, regarded as a function of n_z^2 is a concave-upward parabola. The inequality will therefore be satisfied if n_z^2 is greater than the largest zero of this function which requires

$$n_z^2 > \max_{\tilde{n}<1}\left\{K_{\perp} + \frac{K_x^2(K_{\parallel}+K_{\perp}) + \sqrt{K_x^4(K_{\parallel}+K_{\perp})^2 - \left(K_x^4 - 4K_{\parallel}K_{\perp}K_x^2\right)(K_{\parallel}-K_{\perp})^2}}{(K_{\parallel}-K_{\perp})^2}\right\}.$$

Substituting Eq. 5, neglecting terms of order m/M compared with unity, and using the fact that $\beta/a^2 \ll 1$ yields

$$n_z^2 > \max_{\tilde{n}<1} \left\{ 1 - \left(1 - \frac{\beta}{a}\right)\tilde{n} + \sqrt{\frac{4\beta}{a}(1-\tilde{n})\left(\tilde{n} - \frac{1}{a}\right)} \right\}.$$

Since $\beta \lesssim a$, and $a \gg 1$, a sufficient condition for eliminating complex waves is

$$n_z^2 > 1 + \sqrt{\frac{\beta}{a}}. \tag{6}$$

For Alcator, this requires $n_z^2 > 1.3$, which is a little less restrictive than the condition given by Stix, which for this case is $n_z^2 > 2\left(1 + \frac{\beta}{a}\right)$. When Eq. 6 is satisfied, the solution of the dispersion equation has the appearance shown in Fig. VI-9c. Note that for very small $\tilde{n}$, a small region of evanescence is found in the resonant mode because at zero density evanescent waves must occur for $n_z > 1$. This may be investigated by neglecting K_x^2 (which is proportional to $\tilde{n}^2$) in Eq. 1 and then factoring to obtain

$$\left(n_x^2 + n_z^2 - K_\perp\right)\left(n_x^2 K_\perp + K_\parallel\left(n_z^2 - K_\perp\right)\right) = 0. \tag{7}$$

The mode of interest is that associated with the second factor. Hence, for very low density,

$$n_x^2 = -\frac{K_\parallel\left(n_z^2 - K_\perp\right)}{K_\perp}. \tag{8}$$

For $\tilde{n}$ greater than a^{-1}, $K_\parallel < 0$, and the mode becomes propagating. For moderate n_z^2 ($\gtrsim 2$), n_x^2 is adequately given by Eq. 8 right into the resonance region, providing $\omega_{pe}^2 \ll \omega_{ce}^2$. In fact, near resonance, from Eq. 1,

$$n_x^2 = -\frac{K_\parallel\left(n_z^2 - K_\perp\right) - K_x^2}{K_\perp},$$

which is equivalent to Eq. 8, since $K_x^2 \ll K_\parallel$ ($\beta \ll a$).

To summarize, we find that addition of a relatively small component of wave number parallel to the field allows the mode to propagate parallel to the density gradient and into the resonant zone. Although there is a region of evanescence, it is very small, occurring for $\tilde{n} < a^{-1}$ or $n \lesssim \frac{m}{M} n_o$, where n_o is the resonant density.

Finally, let us inquire into the polarization of this mode. The fields are given by

$$E_z = \frac{n_z n_x}{n_x^2 - K_{\parallel}} E_x \tag{9a}$$

and

$$E_y = \frac{-K_x}{n_x^2 + n_z^2 - K_{\perp}} E_x. \tag{9b}$$

In the low-density limit for which the dispersion equation factors as given in Eq. 7, the modes separate with only E_y nonzero for the mode corresponding to the first factor, and only E_x and E_z nonzero for the mode associated with the second factor. As the latter mode is the resonant mode, this implies that the launching structure should create an electric field parallel to the plane determined by $\bar{k}$ and $\bar{B}$. This is somewhat surprising because, with $n_z^2 = 0$, the resonant mode (extraordinary mode) has E perpendicular to $\bar{k}$ and $\bar{B}$. Physically this is due to the profound influence of electron currents flowing parallel to the magnetic field which are induced when $\bar{k}$ has a component parallel to $\bar{B}$.

Coupling Impedance

These results suggest that the heating mode should be launched from a coupling structure having most of its spectral energy in wave numbers such that $n_z^2 > 1$. Also, the polarization should be such as to launch a mode with $\bar{E}$ parallel to the plane of $\bar{B}$ and $\bar{k}$. We shall now calculate the impedance of such a structure, in order to see if launching from an electromagnetic structure is feasible.

The problem to be considered is illustrated in Fig. VI-10, which shows a cold

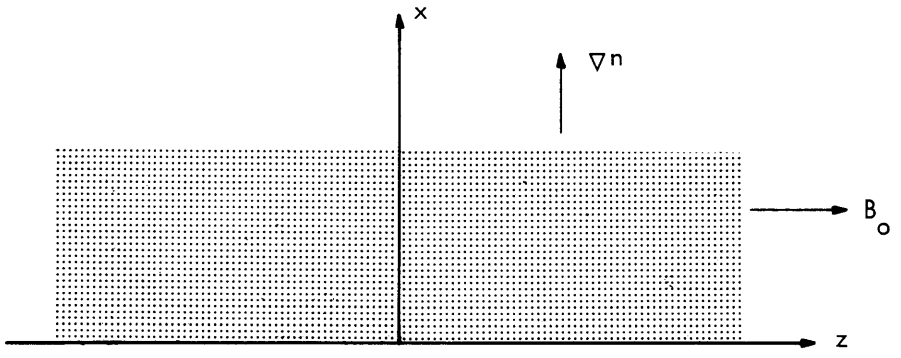

Fig. VI-10. Schematic illustration of the problem.

plasma bounded by a plane at x = 0 along which the electric field $E_z(z, x=0)$ is specified. We assume $E_z = E_o e^{-ik_z z}$, where $\frac{k_z c}{\omega} > 1.15$, in accordance with the accessibility condition. We also assume that the density increases monotonically from zero at the plane x = 0 to a maximum value exceeding that at which hybrid resonance will occur. The problem is to solve for the electric field, subject to a radiation condition, that is, energy propagating toward the resonance zone where it will be absorbed by some unspecified process.

The complete problem is far too difficult to solve analytically, so we shall attempt an approximate solution. Our approach will be to neglect the K_x term in the dielectric tensor, which allows dicoupling of the two modes according to their initial polarization. This seems justified, since K_x can be ignored in the local dispersion relation for the resonant mode. If necessary, corrections arising from the K_x term could be calculated, but we shall not attempt this here.

By neglecting K_x, we can derive the following equation for E_z:

$$E_z'' - k_o^2 K_{\parallel}\left(\frac{n_z^2}{K_\perp} - 1\right)E_z + k_o^2 \frac{n_z^2 K_\perp'}{n_z^2 - K_\perp} E_z' = 0, \tag{10}$$

where primes refer to derivatives with respect to x and $k_o = \omega/c$. We neglect the last term in this equation since it is of order $\left|\frac{\nabla n}{k_x n}\right|^{-1}$, which will turn out to be much less than one. The WKB solution to Eq. 10 will then be adequate except where $K_{\parallel} \to 0$ and $K_\perp \to 0$. The latter point is the resonance, and it is known that the solution near this point is a single propagating wave, propagating into the resonance layer and being completely absorbed there. Within the framework of cold-plasma theory, this result is independent of the absorption mechanism. We expect hot-plasma theory to reveal a conversion to an extremely short wavelength ion plasma mode, along the lines suggested by Stix. At present, we do not concern ourselves with the absorption mechanism, but concentrate on the solution in the neighborhood of $K_\perp = 0$, subject to the boundary conditions of specified E_z at x = 0 and outgoing waves, in the group velocity sense, on the propagating side of the cutoff layer.

In the region where $K_\perp = 0$, the density will be approximated as <u>linear</u>, so that $K_{\parallel} = K_{\parallel o}'(x-a)$, where a is the point at which $K_{\parallel} = 0$. Also, $K_\perp$ can be taken to be unity here because $\tilde{n} \sim \frac{1}{a} \ll 1$. Then Eq. 10 becomes

$$E_z'' + \nu^2 (x-a) E_z = 0, \tag{11}$$

where $\nu^2 = -k_o^2 K_{\parallel o}'\left(n_z^2 - 1\right)$. The general solution to Eq. 11 is $E = e\left(\nu^{2/3}(x-x_o)\right)$, where

$$e(z) = K_1 Ai(-z) + K_2 Bi(-z),$$

and Ai and Bi are the Airy functions. For negative real arguments these functions have the asymptotic forms

$$Ai(-z) \rightarrow \frac{1}{\pi^{1/2} z^{1/4}} \sin(\phi+\pi/4)$$

$$Bi(-z) \rightarrow \frac{1}{\pi^{1/2} z^{1/4}} \cos(\phi+\pi/4),$$

with $\phi = \frac{2}{3} z^{3/2}$. Since the local solution to Eq. 10 is a backward wave, the appropriate boundary condition for large x is $K_1 = jK_2$. Application of the boundary condition of prescribed field amplitude at x = 0 then determines K_1 and K_2 uniquely. Of more interest is the coupling impedance, η, defined as the ratio of E_z to $-H_y$ at the boundary, x = 0. From Maxwell's equations H_y is found to be related to E_z by

$$H_y = \frac{1/j\omega\mu_o}{1 - n_z^2/K_\perp} E_z',$$

so

$$\eta = -\frac{j\omega\mu_o\left(n_z^2-1\right)}{\nu^{2/3}} \frac{Bi(Z) + jAi(Z)}{Bi'(Z) + jAi'(Z)},$$

where $Z = \nu^{2/3} a$. In terms of the parameters,

$$Z = \left[-k_o^2 K'_{\|o} a^3 \left(n_z^2-1\right)\right]^{1/3}.$$

Inserting typical values, we find $Z \sim 10^{-2} - 10^{-1}$. Hence small-argument expansion of the Airy functions is appropriate. Using $Ai(Z) \approx c_1 - c_2 Z + 0(Z^3)$, $Bi(Z) \approx \sqrt{3}\, c_1 Z + 0(Z^3)$, where $c_1 = 0.355$ and $c_2 = 0.259$, we get, to order Z,

$$\eta = -\frac{j\omega\mu_o\left(n_z^2-1\right)}{\left[-k_o^2 K'_{\|o}\left(n_z^2-1\right)\right]^{1/3}} \left[\frac{\sqrt{3}+j}{\sqrt{3}-j}\frac{c_1}{c_2} + Z\right].$$

Hence

$$\text{Re } \eta = \frac{\eta_o\left(n_z^2-1\right)}{\left[-k_o^{-1}K'_{\|o}\left(n_z^2-1\right)\right]^{1/3}} \frac{\sqrt{3}}{2} \frac{c_1}{c_2},$$

where $\eta_o = \sqrt{\mu_o/\epsilon_o} = 377\ \Omega$. Inserting reasonable values for the parameters, Re η turns out to be of the order of 50 Ω. Note that although $K'_{\|o}$ is not known accurately, the third power makes the impedance relatively insensitive to the density scale length. We note also that the impedance is capacitive, having an angle of $-30°$ for $Z \ll 1$.

Finally, we calculate the electric field, given a boundary condition of specified electric field at x = 0. We have

$$E = K_2(\text{Bi}(\nu^{2/3}(a-x)) + j\text{Ai}(\nu^{2/3}(a-x))).$$

Setting x = 0 and $E_z(z, x=0) = E_o e^{-ik_z z}$, we have

$$K_2 = \frac{E_o e^{-ik_z z}}{(\sqrt{3}+j)c_1}.$$

The asymptotic form then becomes

$$E \to \frac{E_o e^{-ik_z z}}{(\sqrt{3}+j)\, c_1 \pi^{1/2}} \frac{1}{\nu^{1/6}(x-a)^{1/4}} e^{j2/3\nu(x-a)^{3/2}}$$

$$= \frac{E_o e^{-ik_z z}\, \nu^{1/3}}{(\sqrt{3}+j)\, c_1 \pi^{1/2}} \frac{1}{k_x^{1/2}} e^{j\int_a^x k_x dx}, \qquad (12)$$

where $k_x = \nu(x-a)^{1/2}$, which is recognized as the WKB form.

Propagation from a Gap

As we have mentioned, the ultimate energy absorption mechanism is still open to question. Even before the energy propagates into the resonance region, it is possible for the pulse to propagate in a rather tortuous path. This is a manifestation of the fact that the group velocity of this mode turns out to be perpendicular to the phase velocity. Since the phase velocity is nearly perpendicular to the magnetic field, the group or energy velocity is nearly parallel to the field. This observation is a warning of the

somewhat surprising result that the energy propagates a long distance parallel to the magnetic field before being absorbed at the resonance layer.

Let us first calculate the group velocity $\overline{V}_g$. In anisotropic media, $\overline{V}_g$ is given by $\partial\omega/\partial\overline{k}$. From Eq. 8,

$$k_x^2 = \frac{-K_{||}}{K_\perp} k_z^2 + k_o^2 K_{||}.$$

We have seen that k_z^2 must exceed k_o^2 and also $K_\perp < 1$, so let us neglect the second term to obtain

$$k_x^2 \approx -\frac{K_{||}}{K_\perp} k_z^2, \tag{13}$$

which is recognized as the quasi-static dispersion relation. By carrying out the calculation for group velocity we get

$$\overline{V}_g = \frac{2k_x/k_z}{k_z^2\left(-\frac{K_{||}}{K_\perp}\right)'} (\hat{i}_y \times \overline{k}),$$

with the prime denoting differentiation with respect to ω. Hence the group velocity is perpendicular to the phase velocity. Also, since $(-K_{||}/K_\perp)' < 0$, k_x must be negative so that energy will propagate away from the wall toward the resonant layer. Hence the mode is a backward wave. We note that at resonance, $V_g \to 0$ because, although $k_x^2 \to \infty$, $(K_{||}/K_\perp)' \to \infty$ and dominates k_x^2.

Let us consider this effect in more detail. From Eq. 12 we have, for large x,

$$E = \frac{E(0, k_z)\, \nu^{1/3}}{(\sqrt{3}+j)\, c_1 \pi^{1/2}} \frac{1}{k_x^{1/2}} e^{j\int_{x_o}^{x} k_x dx}$$

Using the dispersion relation (13), and noting that in the same approximation $\nu^{1/3} \sim k_z^{1/3}$, by undoing the Fourier transform, we get

$$E(z, x) = C(x) \left\{ \frac{1}{2\pi} \int_{-\infty}^{o} dk_z \frac{E(0, k_z)}{k_z^{1/6}} e^{jk_z(z-G(x))} \right.$$

$$\left. + \frac{1}{2\pi} \int_{0}^{\infty} dk_z \frac{E(0, k_z)}{k_z^{1/6}} e^{jk_z(z+G(x))} \right\}, \tag{14}$$

where

$$C(x) = \frac{\left(-k_o^2 K'_{\|o}\right)^{1/6}}{(\sqrt{3}+j)\, c_1 \pi^{1/2}} \left(\frac{K_\perp}{-K_\|}\right)^{1/4}$$

and

$$G(x) = \int_{x_o}^{x} \sqrt{\frac{-K_\|}{K_\perp}}\, dx.$$

The first term in braces in Eq. 14 is constant along curves given by

$$z = z_o + \int_{x_o}^{x} \sqrt{\frac{-K_\|}{K_\perp}}\, dx.$$

This curve is precisely that predicted by following the group velocity from point $x = x_o$, $z = z_o$. This is seen to be true because this trajectory is obtained by solving $\bar{dx} \times \bar{V}_g = 0$, or, since $\bar{k}$ is perpendicular to $\bar{V}_g$,

$$\bar{k} \cdot d\bar{x} = k_x\, dx + k_z\, dz = 0.$$

Hence

$$z = \int_{x_o}^{x} \frac{-k_x}{k_z}\, dx + z_o = \int_{x_o}^{x} \sqrt{\frac{-K_\|}{K_\perp}}\, dx + z_o.$$

Similarly, the second term in braces is constant along the curve $z = -G(x) + z_o$. Note that in a uniform plasma these curves are straight lines with slope ~m/M with respect to the magnetic field. This corresponds to "propagation" ~1 1/2 times around the Alcator torus before reaching the resonant layer.

Let us calculate the form of the electric field from Eq. 14. Considering the first term in braces, we wish to find g(u) defined as

$$g(u) = \frac{1}{2\pi} \int_{-\infty}^{0} dk_z\, \frac{E(0, k_z)}{k_z^{1/6}}\, e^{jku}.$$

If the integration were from $-\infty$ to $+\infty$, g(u) would be essentially the inverse Fourier transform of E (the singularity at k = 0 is of no consequence, since E = 0 for

$k_z < k_o$). Let us denote this function f(u). Then it can be shown that

$$g(u) = \frac{1}{2\pi j} \int_C \frac{f(u')}{u - u'} \, du',$$

where the contour C extends from $-\infty$ to $+\infty$, passing above the point u. Hence, for real u,

$$g(u) = \frac{1}{2} f(u) + \frac{j}{2\pi} P \int \frac{f(u')}{(u'-u)} \, du'.$$

For a gap excitation, E(x = 0, z) would be as shown in Fig. VI-11a. Now $E(0, k_z)$ is the Fourier transform of E(0, z), but void of wave numbers less than k_o, since these

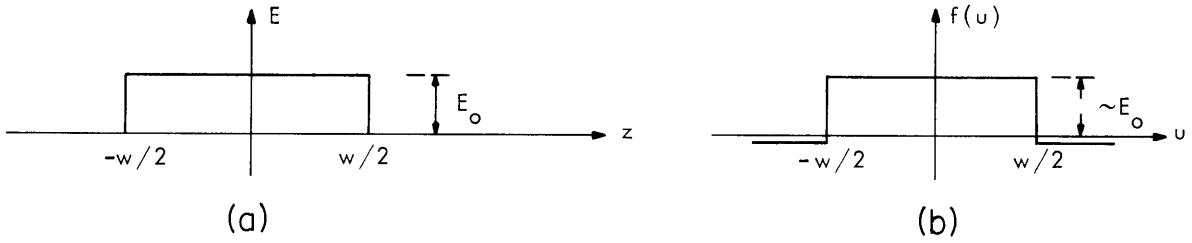

Fig. VI-11. (a) A gap electric field and (b) its appearance after low wave-number components have been removed.

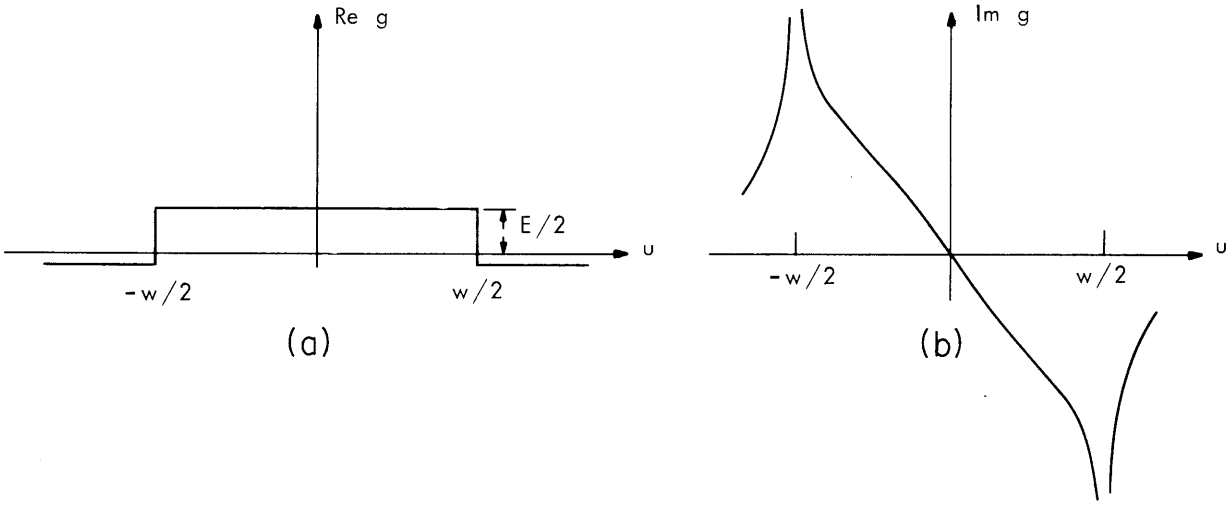

Fig. VI-12. (a) Real and (b) imaginary parts of the asymptotic electric field resulting from the excitation shown in Fig. VI-11a.

wave numbers cannot propagate. For $k_o W \ll 2$, that is, $W \ll \lambda$, this has the effect of removing a small constant component from E, so that the function f(u) has the appearance shown in Fig. VI-11b (it becomes oscillatory for $u > \lambda$). Consequently, g(u) is as shown in Fig. VI-12. For this excitation, we find the presence of a logarithmic singularity in the electric field. Similar effects have been predicted previously by Keuhl,[4] and observed experimentally by Fisher and Gould.[5] Hence we anticipate that strong RF fields may pervade the entire torus, even though the excitation is highly localized. Also, the axial electric field strength should be enhanced over its value in the gap, although we would expect the logarithmic singularity predicted here to be washed out by collisional processes. The absorption mechanism and the nature of fields near the resonance layer remain to be investigated.

R. R. Parker

References

1. T. H. Stix, The Theory of Plasma Waves (McGraw-Hill Book Company, New York, 1962).
2. T. H. Stix, Phys. Rev. Letters 15, 878 (1965).
3. C. R. Skipping, M. E. Oakes, and H. Schluter, Phys. Fluids 12, 1896 (1969).
4. H. H. Kuehl, Phys. Fluids 5, 1095 (1962).
5. R. K. Fisher and R. W. Gould, Phys. Rev. Letters 22, 1093 (1969).